Article:
Bauer, KW, Cole, DB, Asael, D et al. (2019) Chromium isotopes in marine hydrothermal sediments. Chemical Geology, 529. 119286. ISSN: 0009-2541

https://doi.org/10.1016/j.chemgeo.2019.119286

Chromium isotopes in marine hydrothermal sediments

Kohen W. Bauer[1,2], Devon B. Cole[3†], Dan Asael[3], Roger Francois[1], Stephen E. Calvert[1], Simon W. Poulton[4], Noah J. Planavsky[3], Sean A. Crowe[1,2,*]

[1]Department of Earth, Ocean and Atmospheric Sciences, The University of British Columbia 2020 - 2207 Main Mall, Vancouver, British Columbia V6T 1Z4, Canada

[2]Department of Microbiology and Immunology, Life Sciences Centre, The University of British Columbia, 2350 Health Sciences Mall,
Vancouver, British Columbia, V6T 1Z3, Canada

[3]Department of Geology and Geophysics, Yale University, 210 Whitney Ave., New Haven CT 06511, USA

[4]School of Earth and Environment, University of Leeds, LS2 9JT, United Kingdom

[†]Current address: Georgia Institute of Technology, Department of Earth and Atmospheric Sciences, Atlanta, GA USA.

*Corresponding author sean.crowe@ubc.ca

Abstract- Hydrothermal chromium (Cr) cycling contributes to marine Cr inventories and their Cr isotopic composition, yet Cr isotope effects associated with this cycling remain poorly documented. Here we determine the distribution, isotopic composition, and diagenetic mobility of Cr in hydrothermal sediments from the distal flank of the South East Pacific Rise (SEPR, DSDP-site 598). We find that Cr is primarily associated with the metalliferous iron (oxyhydr)oxide and detrital components of the sediment (0.4 – 3.6 mg kg^{-1}), whereas Cr concentrations are much lower in the dominant carbonate phase (<0.03 ± 0.2 mg kg^{-1}). The Cr:Fe ratio of the metalliferous component, however, decreases with increasing depth below the sediment water interface, with an apparent loss of >80% Cr from the sediment relative to Fe. We propose this loss is tied to oxidation of authigenic Cr(III) to Cr(VI) followed by diagenetic remobilization and efflux from the sediment pile. The bulk $\delta^{53}Cr$ composition of the SEPR sediments is isotopically light (-0.24 to -0.57 ± 0.05‰) and the authigenic $\delta^{53}Cr$ is as light as -1.2 ± 0.2‰, and we argue that this light Cr isotopic composition results from the partial reduction of oxic seawater-bearing Cr(VI) by reduced hydrothermal vent fluids enriched in $Fe(II)_{aq}$. Diagenetic oxidation of the reactive Cr pool by Mn-oxides and loss of Cr(VI) from the sediment may further deplete the sediment in ^{53}Cr during diagenesis. The $\delta^{53}Cr$ composition of the detrital Cr fraction of the sediment (average $\delta^{53}Cr$ composition = -0.05 ± 0.04‰) falls within the igneous silicate earth (ISE) range, revealing that detrital Cr delivered to this region of the Pacific ocean is unfractionated, and has carried a relatively constant $\delta^{53}Cr$ composition over the last 5.7 million years. Together our results show that light $\delta^{53}Cr$ compositions in hydrothermal sediments are imparted through a combination of processes previously overlooked in the marine Cr biogeochemical cycle, and that the $\delta^{53}Cr$ composition of such sediments may provide a rich source of information on paleo-marine redox conditions.

1.0 Introduction

Chromium (Cr) isotope ratios are emerging as proxy that can track the evolving redox state of the ocean-atmosphere system over geologic time-scales (Cole et al., 2016; Crowe et al., 2013; Frei et al., 2011; Gueguen et al., 2016; Holmden et al., 2016; Planavsky et al., 2014). The simplest application of the Cr isotope system uses large amplitude shifts in the Cr isotopic composition of sedimentary rocks, like banded iron formations (BIF) and ironstones, together with shales and limestones to record the onset of Cr redox cycling, which is indicative of the presence of oxygen in Earth's surface environments (Bonnand et al., 2013; Cole et al., 2016; Crowe et al., 2013; Frei et al., 2009; Gilleaudeau et al., 2016; Planavsky et al., 2014). However, more detailed insight into Cr isotope systematics could enable more nuanced applications of the proxy. For example, improved knowledge of the distribution of Cr isotopes in a wider range of sedimentary reservoirs that serve as Cr repositories and archives of past Earth surface chemistry is essential for the development of a global isotope mass balance. Further knowledge of the modern Cr cycle also provides a means to test many of the assumptions built into the current interpretation of the Cr isotope record.

Our emerging picture of the global Cr cycle is illustrated schematically in Figure 1. Chromium resides in the continental crust bound in its relatively low solubility trivalent redox state Cr(III), and is hosted in silicate and oxide minerals (Fendorf, 1995; Oze et al., 2004). In the modern Earth system, with O_2 comprising 21% of the atmosphere, this Cr is liberated to runoff predominantly through oxidative weathering at Earth's surface, which produces Cr(VI) from Cr(III) through heterogenous solid-state catalysis by Mn-oxides. (Rai et al., 1989; Schroeder and Lee, 1975). It has also been suggested that Cr(III) may also be oxidized by H_2O_2 in the local absence of O_2 in serpentinizing systems (Oze et al., 2016), however a strong oxidant like O_2 is likely required to generate this peroxide or other oxidants of Cr at the outset. Riverine transport of Cr(VI) produced during oxidative weathering sustains the largest Cr flux to the modern oceans (Jeandel and Minster, 1984; McClain and Maher, 2016; Reinhard et al., 2013). Once in the oceans, this Cr(VI) is likely removed from seawater via reduction, by an as yet unknown diversity of electron donors, to Cr(III), which in turn is scavenged by settling particles and ultimately deposited in sea-floor sediments (Dossing et al., 2011; Ellis et al., 2002; Gueguen et al., 2016; Kitchen et al., 2012; Reinhard et al., 2014). A fraction of Cr may also be delivered to

81 the oceans via rivers as Cr(III), partly stabilized as Cr(III)-organic complexes, or dissolved in
82 low pH systems (Fendorf, 1995; Rai et al., 1989; Yusof et al., 2007).
83 The contribution of hydrothermal systems to the marine Cr inventory remains poorly
84 constrained, and may represent a net source or sink of Cr in the global marine Cr mass balance.
85 Previous work suggests that Cr from hydrothermal vents represents ~0.02% of the Cr riverine
86 flux, or 12 x 10^6 mol yr^{-1}, implying that the contribution of Cr to seawater from hydrothermal
87 fluids is likely very small (Reinhard et al., 2013). While vent fluids emit Cr(III) derived from
88 acid dissolution of basaltic ocean crust, much of this Cr(III) is scavenged by Fe (oxyhydr)oxide
89 particles formed during the mixing of Fe(II)-laden vent fluids with ambient oxygenated seawater
90 (Dymond and Roth, 1988; Feely et al., 1996; Rudnicki and Elderfield, 1993; Sander and
91 Koschinsky, 2000). Deposition of these Fe (oxyhydr)oxides may thus quantitatively capture the
92 vent flux of Cr, which is then largely deposited in proximal and distal hydrothermal sediments
93 (Trocine and Trefry, 1988). However, given the typically strong vent flux of ferrous Fe – a
94 potent reductant of Cr(VI) – precipitation of hydrothermal Fe (oxyhydr)oxides particles may also
95 capture a fraction of seawater Cr(VI), rendering vent systems a net sink for seawater Cr (Trocine
96 and Trefry, 1988). While the fate of Cr in these particles remains unknown, long distance
97 transport of hydrothermal Fe and associated elements may distribute hydrothermal Cr over long
98 distances in the oceans. Cr(III) associated with Fe (oxyhydr)oxides generally has a low solubility
99 (e.g., Oze et al. (2004)) and, therefore, deposition of Cr in hydrothermal sediments may lead to
100 effective and quantitative burial of hydrothermal Cr with such phases. It has also been suggested,
101 however, that there is extensive Cr remobilization in surficial continental-margin Mn-oxide
102 bearing sediments (Shaw et al., 1990), which implies the potential for Cr remobilization from
103 Mn-oxide bearing hydrothermal sediments. Additional information on the fate of Cr deposited in
104 hydrothermal sediments is thus needed to better constrain the role of vent systems in the marine
105 Cr cycle.
106 Chromium isotopes are fractionated during redox reactions. During oxidative weathering,
107 the resulting Cr(VI) is enriched in the ^{53}Cr (heavy) isotope through a possible combination of
108 Cr(III) oxidation to Cr(VI) and partial re-reduction of Cr(VI) (Crowe et al., 2013; Zink et al.,
109 2010). Despite current uncertainty around the precise mechanism for this fractionation, heavy
110 δ^{53}Cr(VI) is exported from the weathering environment in runoff, leaving Cr(III) in the residual
111 soil isotopically light (^{53}Cr depleted) (Crowe et al., 2013; D'Arcy et al., 2016; Frei et al., 2011;

112 Frei et al., 2009). Oxidative weathering thus sets the heavy $\delta^{53}Cr$ composition observed in some
113 rivers (e.g. D'Arcy et al. (2016); Frei et al. (2009); Wu et al. (2017)), and contributes to the
114 heavy isotopic composition of seawater (modern values lie between ~ 0.5 and 1.5‰, Bonnand et
115 al. (2013); Scheiderich et al. (2015). On the other hand, dissolution of Cr(III), unless mediated by
116 strongly complexing organic acids (see Saad et al. (2017)), is unlikely to be associated with large
117 isotope fractionation (Crowe et al., 2013; Konhauser et al., 2011). Given that acid dissolution of
118 basalt provides Cr to vent fluids, the efflux of Cr(III) from hydrothermal vent waters is expected
119 to carry an isotopic signature no different from the igneous silicate earth (ISE), -0.12 ± 0.10‰
120 (Schoenberg et al., 2008). As a result, Cr(III) escaping removal via Fe (oxyhydr)oxide particle
121 scavenging in the vicinity of vents, would likely contribute a Cr isotope flux indistinguishable
122 from ISE to the marine Cr inventory, with potential to partly offset heavy signals imparted
123 through the riverine influx of Cr(VI) (Crowe et al., 2013; Schoenberg et al., 2008). Hydrothermal
124 Cr(III) precipitates, however, might also be expected to carry a lighter but variable Cr isotopic
125 composition, if diagenetic reactions remobilized Cr as result of partial oxidation or, if
126 hydrothermal particles captured seawater Cr(VI) through partial reduction.
127 To assess Cr deposition and cycling in hydrothermal settings we have determined the
128 abundances and distribution of Cr, Mn and Fe, together with Cr isotope ratios, from the western
129 distal flank of the South East Pacific Rise (SEPR), one of the fastest spreading centres on the
130 ridge crest system with rates of up to 14.5 cm yr^{-1} (Lyle, 1986). Three sediment cores from the
131 SEPR at DSDP sites 598, 599 and 600 were examined, with a focus on the more distal site 598,
132 which is currently ~1130 km west of the ridge crest. These sites have collected particulate
133 hydrothermal materials derived from the crest of the SEPR spreading center and transported by
134 westward-flowing deep-ocean circulation. Sequential extraction techniques were employed to
135 target Cr in different mineral phases of the sediment, and we used the molar ratios of Cr, Fe and
136 Mn to evaluate post-depositional alteration. We then assessed the implications of this
137 redistribution for marine Cr budgets, ocean isotope mass balance, and the use of Cr isotopes as a
138 proxy for the oxygenation state of the oceans.
139
140 2.0 Methodology
141 The three sediment cores used in this study were collected during DSDP Leg 92 in 1984.
142 They were previously used by Lyle (1986), to investigate the bulk sediment major element

143 geochemistry and the history of hydrothermal sedimentation on the south-eastern flank of the
144 SEPR. Poulton and Canfield (2006) conducted a study of the association of P with Fe
145 (oxyhydr)oxides and other phases in the upper 5.5 m at site 598. This site represents the most
146 distal location from the ridge crest and via seafloor spreading is now located 1130 km from the
147 active vent. Using splits from the same sample suite (Poulton and Canfield (2006)) we
148 constructed a profile from the core surface to 5.5 m depth, corresponding to an age of 5.5 Myr at
149 5.5 m depth (Poulton and Canfield, 2006). To investigate vent particle alteration processes, Mn-
150 oxide and Fe concentrations were determined in 5 samples across the top 20 cm of cores from
151 the other sites (599 and 600), which are closer to the ridge crest, allowing us to track chemical
152 changes in the Mn:Fe ratio of surface sediments in relation to the proximity to the ridge crest.
153 The sediments at all three sites are reported to be compositionally simple, mainly comprising two
154 phases, namely foraminferal and nannofossil carbonates (37- 95%) and metalliferous
155 hydrothermal precipitates (3-40% of bulk sediment) (Barrett et al., 1987). Importantly, the
156 sediments contain only small amounts of lithogenous detrital material as the sample locations are
157 well removed from continental input sources (Barrett et al., 1987).
158
159 2.1 Chemical extraction techniques
160 A selective extraction scheme was used to quantify Cr in the different operationally
161 defined phases of the hydrothermal sediment. Figure 2 is a schematic illustration of these
162 procedures. We employed four different leaches in sequence, adapted from the procedures of
163 Poulton and Canfield (2005), and two separate bulk digests. Table 1 contains a detailed
164 breakdown of our leaching procedures and how they relate to the nomenclature employed in
165 Poulton and Canfield (2006). The first leach in sequence (L_{Carb}) targeted the carbonate fraction.
166 Powdered samples of ~200 mg were weighed into centrifuge tubes and leached with 10% acetic
167 acid (Barrett et al., 1987). The acid addition was in excess of that needed to dissolve 200 mg of
168 pure $CaCO_3$. Samples were placed on a shaker for 4 hours and subsequently centrifuged. An
169 aliquot of supernatant was taken and diluted for Cr concentration analyses via inductively
170 coupled plasma mass spectrometry (ICP-MS) and inductively coupled plasma optical emission
171 spectrometry (ICP-OES). A subset of sediment samples were analysed for total inorganic carbon
172 via coulometry before and after application of the first leach to ensure all $CaCO_3$ was
173 successfully dissolved. Following removal of carbonate, the residual sediment was subjected to

the second leach in sequence, which targets poorly crystalline Fe-(oxyhydr)oxide phases (lepidocrocite, ferrihydrite) (Thamdrup et al., 1994) using trace metal grade 0.5 N HCl (Thamdrup et al., 1994) (L_{HFO}, which is broadly analogous to the Fe_{HFO} fraction in Poulton and Canfield (2006)). The supernatant was decanted, filtered, and diluted for measurement via ICP-MS.

Following the L_{HFO} extraction, the remaining sediment contained more crystalline metal (oxyhydr)oxides as well as refractory detrital components. In order to differentiate between the more crystalline authigenic metal (oxyhydr)oxides (e.g., goethite and hematite) and refractory detrital minerals, we first subjected the residual sediment to 0.35 M acetic acid/0.2 M Na-citrate buffered Na-dithionite leach for 2 hours (L_{GOE}, which targets minerals such as goethite and hematite, and is referred to as the Fe_{GOE} fraction in Poulton and Canfield (2006)). The supernatant was decanted following centrifugation, filtered, and diluted for measurement via ICP-OES. We did not directly determine the Cr concentration of this sediment phase analytically due to matrix effects of the L_{GOE} extract in the quadrupole ICP-MS, and we thus estimated the Cr concentration of this leach using a mass balance approach (see Section 3.2 below). Following the L_{GOE} extraction a small volume of greyish residual sediment remained, comprising the refractory component of the sediment (not extractable in the L_{Carb}, L_{HFO} or L_{GOE} fractions). We leached the residual sediment from L_{GOE} with near boiling 6 N HCl for 24 h (L_{Sil}, analogous to the Fe_{Sil} fraction in Poulton and Canfield (2006)). Again, samples were centrifuged and an aliquot of the supernatant was removed and diluted for analysis via ICP-MS and ICP-OES. We also performed a separate bulk digest with 6 N HCl on 200 mg sediment by adding 10 mL of acid in sealed centrifuge tubes (L_{6NHCl}). Again, samples were centrifuged and an aliquot of the supernatant was removed and diluted for analysis via ICP-MS and ICP-OES.

The reactive Mn and Fe (oxyhydr)oxide content in sediments from the upper 10 cm at sites 599 and 600, and from 5.5 m at site 598, were determined following the method of Neaman et al. (2004) and Chao (1972). Samples of 7.5 mg were weighed into centrifuge tubes and leached for 2 h with 0.1 M hydroxylamine hydrochloride (L_{MnOx}). The amount of NH_2OH-HCl added was in a 1:2000 solid – solution ratio. Samples were centrifuged and an aliquot of supernatant was taken for analysis by ICP-OES. Reaction time was limited to 2 h to restrict dissolution of poorly crystalline iron-oxides (Neaman et al., 2004). Iron concentrations in these extracts accounted for only 0.01% of the bulk Fe in the sediments.

205

206 2.2 Analytical methods

207 Chromium concentrations in our leachates were determined by ICP-MS, while major
208 elements Al, Fe and Mn were determined by ICP-OES. The error on [Fe] measurements was ±
209 8% RSD based on the difference between triplicate measurements, and the detection limit,
210 calculated as three times the standard deviation of the blank (n = 5) was 8 ppb in solution and
211 roughly 35 mg kg^{-1} in the solid phase based on our dilutions. The error on our ICP-OES [Mn]
212 measurements was ± 5% RSD based on the difference between triplicate measurements, and the
213 detection limit, calculated as three times the standard deviation of the blank (n = 5) was 6 ppb in
214 solution and roughly 30 mg kg^{-1} in the solid phase based on our dilutions. The error on [Cr]
215 measurements is ± <1% RSD based on the difference between triplicate measurements, and the
216 detection limit, calculated as three times the standard deviation of the blank (n = 5), translates to
217 0.028 mg kg^{-1} in the solid phase.

218

219 2.3 XRD analysis

220 We used quantitative X-ray diffraction (qXRD) methods on 6 bulk sediment samples to
221 determine the sediment mineralogy. The samples were smear mounted with ethanol on non-
222 diffracting silica plates. Continuous-scan X-ray powder-diffraction data were collected over a
223 range 3-80°2θ with CoKα radiation on a Bruker D8 Focus Bragg-Brentano diffractometer
224 equipped with an Fe monochromator foil, 0.6 mm (0.3°) divergence slit, incident- and diffracted-
225 beam Soller slits and a LynxEye detector. The long fine-focus Co X-ray tube was operated at 35
226 kV and 40 mA, using a take-off angle of 6°. We analyzed the X-ray diffractograms using the
227 International Centre for Diffraction Database PDF-4 and Search-Match software by Bruker. X-
228 ray powder-diffraction data of the samples were refined with Rietveld program Topas 4.2
229 (Bruker AXS).

230

231 2.4 Cr purification and isotope ratio determination

232 Chromium isotope ratios were determined on a Multi-Collector Inductively-Coupled
233 Plasma Mass Spectrometer (MC-ICP-MS, Thermo Neptune) at the Yale Metal Geochemistry
234 Center using a double-spike correction for isotope fractionation during column chemistry and
235 instrumental mass bias. The spike was added to acid splits after the digestion procedure (bulk

sediment 6 N HCl digestion, L_{6NHCl} leachate as well as the L_{GOE} and L_{Sil} 6 N HCl digestion performed sequentially). Although isotope effects due to leaching in Na-dithionite and 6 N HCl have not been tested directly, we do not expect any measurable isotope fractionation during acidic digestions of Cr, even at higher acid molarity (see Crowe et al. (2013) and Reinhard et al. (2013)). We note that previous studies on Fe isotope ratios in rocks and sediments have also shown that there appears to be no isotope effect during proton-promoted acid leaching of Fe oxides, which is in contrast to ligand promoted dissolution (Wiederhold et al., 2006). We used three separate column separations (Reinhard et al., 2014; Schoenberg et al., 2008) to ensure complete removal of Fe, Ti, and V during chemical purification. Initially, a split of the 6 N HCl sample solution was spiked, evaporated to dryness, and the residues brought up in 1 N HCl. The amounts of ^{50}Cr-^{54}Cr double-spike (^{50}Cr/^{52}Cr = 462.917, ^{53}Cr/^{52}Cr = 0.580, ^{54}Cr/^{52}Cr = 354.450, calibrated in the Department of Geology, University of Illinois at Urbana-Champagne and added as Cr(III)), were adjusted so that the spike/sample ratio (i.e., $(^{54}Cr)_{spk}/(^{52}Cr)_{smp}$) was 0.5. Prior to the first column step (AG1-X8 anionic resin, 100-200 mesh), Cr(III) was oxidized to Cr(VI) using potassium peroxidisulfate (heating the samples for 2 h at 110 °C). The AG1-X8 resin was cleaned with mQ water, 3 N HNO_3 and 6 N HCl. The matrix was eluted with 24 ml of 0.2 N HCl and 4 ml 2 N HCl, with Cr subsequently reduced with 5% H_2O_2 and eluted with 5 ml of 2 N HNO_3. The second step removes traces of Fe that may remain after the first elution. Microcolumns were filled with 0.2 ml AG1-X8 resin. The columns were cleaned using mQ water and 3 N HNO_3, and samples were loaded and collected with 1.2 ml of 6 N HCl. Traces of Ti are often left after the first two column steps. Therefore, as the last step, a cation resin AG50W-X8 (200-400 mesh) was used to ensure complete Ti and Cr separation. The resin was cleaned with mQ water, 3 N HNO_3 and 6 N HCl, followed by sample loading in 3 ml of 0.5 N HNO_3 and by matrix elution with 1 ml of 0.5 N HNO_3, 2 ml of 0.5 N HF and 6 ml of 1 N HCl. Cr was collected after elution with 5 ml of 1.8 N HCl.

Chromium isotopes were run in high-resolution mode to resolve polyatomic interferences such as $^{40}Ar^{12}C^+$, $^{40}Ar^{14}N^+$ and $^{40}Ar^{16}O^+$. Although our chemical procedure results in nearly complete removal of Fe, Ti and V, these elements were monitored by measuring ^{56}Fe, ^{49}Ti and ^{51}V, and samples were corrected for potential interferences of ^{54}Fe on ^{54}Cr, as well as ^{50}Ti and ^{50}V on ^{50}Cr. Samples at a concentration of ~100 ng/g were introduced into the plasma with a PFA μFlow nebulizer (~50 μL/min) coupled with an Apex IR (Elemental Scientific) without

additional N_2 gas or membrane desolvation. With a standard sample cone and X skimmer cone under high-resolution mode, the sensitivity obtained was ~3×10^{-10} A ^{52}Cr on 100 ng/g solution. All ion beams were measured on faraday detectors. The double-spike data reduction model is based on the iterative method described by Siebert et al. (2001). A spiked Cr isotope standard NIST SRM 979 was measured bracketing every three natural samples to ensure machine stability. Chromium isotope ratios are reported relative to bracketing standards using conventional delta notation ($\delta^{53}Cr = [(^{53}Cr/^{52}Cr)_{sample}/(^{53}Cr/^{52}Cr)_{NIST\text{-}979} - 1] \times 1000‰$).

External precision is reported as two sigma (2σ) uncertainty, calculated based on duplicate analysis of geological reference materials (GRMs) processed through ion-exchange chromatography columns along with samples (BHVO-2 and Nod-A-1 were systematically processed with 70 samples). The $\delta^{53}Cr$ value for BHVO-2 is -0.11 ± 0.07‰ (n = 3), which is similar to published values in the literature for BHVO-1 (geostandard collected at the same location as BHVO-2) (Schoenberg et al., 2008), and Nod-A-1 yielded a $\delta^{53}Cr$ value of 0.08 ± 0.05‰ (n = 4). Sample duplicates, including column procedure duplicates, digested duplicates, and replicate measurements on the MC-ICP-MS revealed a 2σ uncertainty similar to that determined for GRMs, i.e. ≤ 0.09‰ and an average duplicate offset of 0.043‰. Measurement precision is calculated via replicate measurements of the isotopic standard NIST SRM 979 during each analytical session (two standards bracket every sample), and 2σ values are better than 0.04‰. In addition, a two-standard deviation of the mean (2se) was systematically calculated using the 50 cycles of measurement obtained for each sample during MC-ICP-MS analysis, and was generally 0.04-0.06‰ on the delta values. This precision and accuracy are comparable to long term means at the Yale Metal Geochemistry Center.

3.0 Results

3.1 Mineralogical analyses

Quantification of the relative mineral proportions via qXRD on 6 sub-samples (Table 2) shows that the sediment samples examined here consist almost entirely of calcite and goethite, with very small contributions from crystalline lithogenic minerals (<12%; Table 2), which are inversely proportional to calcite concentration. The detrital fraction is dominated by the feldspar

albite, a felsic mineral, in addition to about 1% hercynite, a spinel phase ($Fe^{2+}Al_2^{3+}O_4$) into which Cr can substitute for Al ($Fe^{2+}Cr_2^{3+}O_4$) (Table 2).

3.2 Site 598 elemental concentrations and Cr mass balance.

Within our sequential leach scheme we first targeted the carbonate phase (L_{Carb}, Table 1). Sediments from site 598 have $CaCO_3$ contents ranging from 42.8 to 93.3 ± 0.1 wt% (Poulton and Canfield, 2006). As noted previously, this fraction is dominated by coccoliths (comprising roughly 85%), with a small (up to 4%) fraction of planktonic foraminifera (Barrett et al., 1987; Lyle, 1986). Carbonate concentrations in the sediment are inversely related to metalliferous phases and this leads to mutual dilution of both authigenic and detrital metals in carbonate rich intervals. Triplicate measurements of Cr concentrations in the carbonate phase were below our detection limit (0.03 mg kg^{-1}) in all of the samples from site 598. These low Cr concentrations in the carbonates contribute to a consistent linear relationship between Cr and Fe in the L_{6NHCl} bulk sediment leachate (Table 1), for samples deeper than 150 cm (Fig. 3) where the average molar Cr:Fe ratio remains nearly constant (Fig. 3). This linear relationship is the result of mixing between Cr deficient carbonate and Cr-rich metalliferous Fe-rich phases. The intercept (0.041 ± 0.2 mg kg^{-1}) provides an independent estimate of the Cr concentration in the $CaCO_3$, which is near the detection limit of our analytical method (0.03 mg kg^{-1}).

The bulk sediment (6 N HCl extractable phases, L_{6NHCl}, Table 4) Fe concentration determined in this study is within ± 5% of the Fe_{TOT} values reported by Poulton and Canfield (2006) and the mass balance of Cr in the individual metalliferous sediment phases is plotted in Fig. 4. Chromium concentrations in the bulk sediment L_{6NHCl} leach range from 0.4 – 3.6 mg kg^{-1}, and are strongly correlated with Fe (Poulton and Canfield, 2006) – the highest Cr concentrations are associated with Fe-rich samples (Fig. 5e), whereas carbonate-rich samples are low in Cr. There is a minor fraction of the Cr contained in the L_{HFO} fraction (Fig. 5b), dominantly comprised of highly reactive hydrous ferric oxide minerals such as ferrihydrite (Poulton and Canfield, 2006), and this is mostly restricted to the upper 150 cm (Fig. 4). The Cr concentration of the L_{Sil} fraction ranges from 0.3 – 2.5 mg kg^{-1} (Fig 5d), indicating that a refractory Cr pool, accounts for 37 – 82% of the total Cr (L_{6NHCl}, Table 4). As discussed in section 2.1, we were unable to analytically determine the Cr concentration of the L_{GOE} leachate, and thus we estimate this via mass balance; $LCr_{GOE} = LCr_{6NHCl} - (LCr_{HFO} + LCr_{Sil}$; Table 3). The majority of Cr in the

site 598 sediments is thus mainly contained in two fractions; the L_{GOE} (Na-dithionite extractable, Table 3) sediment fraction, comprising crystalline Fe-(oxyhydr)oxide mineral phases such as goethite, and the refractory L_{Sil} fractions (Fig. 5c-d and Table 3).

The average Cr:Fe ratio of the sediments is 4.8 x 10^{-5}, with a maximum value of 10.2 x 10^{-5} and minimum value of 1.9 x 10^{-5}. In the upper 150 cm of the sediment pile there is a clear and systematic decrease in the ratio of total Cr:Fe (L_{6NHCl}, Fig. 5j), below which the ratio remains relatively constant (Fig. 5g-h). These more deeply buried intervals have a Cr:Fe ratio (~ 2.0 x 10^{-5}), which is 5.5 times lower than those at the core top (~ 10.2 x 10^{-5}), and 20 times lower than fresh hydrothermal vent plume particles (~ 40 x10^{-5}, Feely et al. (1996), Fig. 6). Within the upper 150 cm, we also observe a decrease in the amount of L_{HFO} extractable Cr, and an increase in L_{GOE} extractable Cr (Fig. 4 and Fig. 5h).

3.3 Mn-oxide concentrations

To directly test the capacity of the SEPR sediments to oxidize Cr, we also determined reactive Mn-oxide concentrations in the sediment. The Mn (oxyhydr)oxide concentrations in the sediment at site 598 follow similar trends to those of bulk Fe_{6NHCl} (Fig. 5f), with a maximum concentration of 3.9 wt% at the sediment water interface. Extractable Mn in the upper 20 cm of sediment at sites 599 and 600 also shows that the total Mn:Fe (oxyhydr)oxide ratio increases with distance from the ridge crest (Table 5).

3.4 Chromium isotopes

Chromium extracted from bulk SEPR site 598 sediments with a 6 N HCl (L_{6NHCl}) leach (Table 4, Fig. 7) has $\delta^{53}Cr$ values that are significantly lower (-0.24 to -0.57‰, 2 tailed t-test p-value = 4 x 10^{-6} at the 95% confidence level) than the ISE (-0.12 ± 0.10‰) and oxic abyssal ocean sediments (0.23 to -0.14‰; Gueguen et al. (2016); Schoenberg et al. (2008)). The bulk L_{6NHCl} leach contains both the authigenic reactive Cr phases (L_{HFO} and L_{GOE}) as well as the refractory Cr (L_{Sil}). There is a general decrease in $\delta^{53}Cr$ with increasing sediment depth and decreasing Cr:Fe ratios (Fig. 7). The lightest $\delta^{53}Cr$ values come from samples below 150 cm. We also determined the Cr isotope composition of four select L_{GOE} samples, comprising authigenic Cr contained in more crystalline Fe mineral phases. The $\delta^{53}Cr$ composition of these samples is very isotopically light relative to the ISE with an average $\delta^{53}Cr$ composition of -1.1 ± 0.1‰ (Fig.

7a). Additionally, we determined the Cr isotope composition of the L_{Sil} sediment fraction, comprising only the refractory sediment phases, of which almost all $\delta^{53}Cr$ values fall within error of the ISE with an average $\delta^{53}Cr$ composition of -0.05 ± 0.04‰ (Table 3, Fig. 7). The L_{Sil} leach was performed after extraction and removal of the more reactive and likely authigenic phases of Cr (L_{HFO} and L_{GOE}), and thus we consider Cr contained in the L_{Sil} fraction to represent detrital Cr. The isotopic composition of the detrital L_{Sil} Cr in site 598 sediments is not significantly different than the ISE composition (2 tailed t-test p-value = 0.26 at the 95% confidence level).

To estimate the Cr isotopic composition of the reactive and likely authigenic component of the site 598 sediment (the sum of L_{HFO} and L_{GOE} extractable Cr), we corrected for detrital Cr with its ISE composition using a mass balance calculation;

$$\delta^{53}Cr_{authigenic} = (\delta^{53}Cr_{measured} - (\delta^{53}Cr_{detrital} * X)) / (1-X) \qquad (1)$$

where $\delta^{53}Cr_{authigenic}$ is the calculated Cr isotopic composition of authigenic Cr, $\delta^{53}Cr_{measured}$ is the bulk Cr isotope composition represented by our L_{6NHCl} leach (Table 4), and $\delta^{53}Cr_{detrital}$ is the Cr isotope composition of the detrital fraction of the sediment, which we take from our L_{Sil} isotope values. X is the fraction of detrital Cr in the Fe_{6NHCl} leach. As described above, the Cr concentration in our L_{Sil} leachates from our sequential extractions is our best estimate of the detrital Cr contribution to the L_{6NHCl} bulk measurements (Tables 3 and 4). The results of our mass balance calculation are shown in (Fig. 7a). We note that there are large uncertainties (0.1 - 0.3‰ SE) on the $\delta^{53}Cr$ composition of the calculated authigenic component that result from error propagation in our mass balance calculation and these are not plotted to maintain figure clarity, but instead are presented in (Table 4). Our calculation demonstrates that once corrected for the contribution from detrital Cr, the $\delta^{53}Cr_{authigenic}$ values of the SEPR sediments are even lighter than the measured L_{6NHCl} bulk Cr isotope compositions. These estimates, furthermore, are within analytical error of the four measured $\delta^{53}Cr$ L_{GOE} samples, which thus satisfies mass balance.

We performed a similar calculation to test whether the isotopic composition of the bulk sediment at site 598 (Cr isotopic composition of the L_{6NHCl} leach; sum L_{HFO}, L_{GOE} and L_{Sil} extractable Cr) can be obtained via mass balance and is similar to our measured $\delta^{53}Cr$ L_{6NHCl} values;

$$\delta^{53}Cr_{Bulk} = (\delta^{53}Cr_{authigenic} * X_{authigenic}) + (\delta^{53}Cr_{detrital} * X_{detrital}) \quad (2)$$

where $\delta^{53}Cr_{Bulk}$ is the calculated Cr isotopic composition of the bulk sediment, $\delta^{53}Cr_{authigenic}$ is the Cr isotopic composition of the authigenic L_{GOE} leach (4 samples), and $X_{authigenic}$ is the fraction of authigenic Cr in the L_{6NHCl} leach. $\delta^{53}Cr_{detrital}$ is the Cr isotope composition of the detrital fraction of the sediment, which we take as our L_{Sil} isotope values. X is the fraction of detrital Cr in the L_{6NHCl} leach. We use the Cr concentration of our L_{Sil} leachates from our sequential extractions as best estimates of the detrital Cr contribution (Table 3). The results of this mass balance calculation are also shown in (Fig. 7a). This calculation demonstrates that for the four samples analyzed, the calculated $\delta^{53}Cr_{Bulk}$ values are the same as the measured L_{6NHCl} δ^{53}Cr compositions within error, satisfying isotopic mass balance and giving further confidence in our conclusion that authigenic Cr buried in the SEPR sediments is isotopically light relative to the ISE and detrital Cr.

4.0 Discussion

4.1 Cr in the carbonate phase

Poulton and Canfield (2006) attribute the variability in metal concentrations in the sediment at site 598 to changes in the accumulation rate of $CaCO_3$ rather than to fluctuations in the deposition rate of the metalliferous hydrothermal component. This biogenic carbonate carries a negligible fraction of the sediment Cr despite the fact that it is the dominant component of the sediment at site 598. We considered the possibility that calcite bound Cr released during the carbonate leach might have been re-adsorbed onto the remaining Fe-phases. Davis and Leckie (1980) found that Cr adsorption to Fe (oxyhydr)oxides is maximal in a pH range of 5-6 and less than 30% below pH 4. Although re-adsorption of calcite bound Cr to Fe-(oxyhydr)oxides during our carbonate leach cannot explicitly be ruled out, our 10% acetic acid leach was at pH ~4, and hence we do not expect adsorption of more than 30%. Modern planktonic foraminifera, furthermore, typically exhibit Cr concentrations between 0.05 and 0.3 mg kg^{-1} (Wang et al., 2017), which is consistent with biogenic carbonates having lower Cr concentrations than limestones (Gilleaudeau et al., 2016). Experimental studies show that Cr(VI) incorporation into calcite (as CrO_4^{2-}) increases with increasing Cr(VI) concentration in solution (Tang et al., 2007).

We applied the partition coefficient (K_d^*) from this experimental work (Tang et al., 2007), where;

$$K_d^* = [Cr(VI)]_{solid}/[Cr(VI)]_{solution} \quad (3)$$

and when $[Cr]_{solution}$ drops below a minimum of 10 mmol l^{-1}, Kd^* reaches a maximum value of ~95. If this value is extended to Cr(VI) concentrations of 1.95 ± 0.15 nmol l^{-1} observed by Jeandel and Minster (1984) in surface waters above the East Pacific Rise, we calculate an expected $[Cr]_{solid}$ of 0.2 mg kg^{-1} in calcite, which is below our detection limit. Together, our observations imply that a negligible fraction of the Cr in SEPR sediments is associated with carbonate phases.

4.2 Oxygenated deep-sea sediments and authigenic Cr

The authigenic Cr in the SEPR sediments has a $\delta^{53}Cr$ isotopic composition that is lighter than other oxygenated marine sediments measured to date. The $\delta^{53}Cr$ composition of the majority of previously measured marine sediments deposited from oxygenated seawater fall within the ISE range (-0.12 ± 0.10‰, Gueguen et al. (2016); Schoenberg et al. (2008)), while ferromanganese nodules accumulating beneath oxygenated seawater are isotopically light (Table 6) (Wei et al., 2018). Together, these yield an average $\delta^{53}Cr$ value of -0.15 ± 0.05‰ for oxic marine sediments. Prior leaching experiments conducted to target the authigenic Cr pool from these sediments also yielded $\delta^{53}Cr$ values that were not statistically different from the bulk sediment (-0.01 ± 0.05‰, Gueguen et al. (2016)). Current data for oxic deep-sea sediments, therefore, suggest that fractionated authigenic Cr pools likely comprise a very minor fraction of the total sediment Cr, and thus the $\delta^{53}Cr$ composition of these sediments reflects a detrital input with composition identical to the ISE (Gueguen et al., 2016; Schoenberg et al., 2008). The sediments at site 598 were also deposited under oxygenated deep-sea conditions yet they contain an appreciable (up to 56%) authigenic component, and in contrast to other oxygenated sediments, are overwhelmingly isotopically light. Similar leaching techniques designed to target authigenic Cr in the SEPR sediments, reveal that this authigenic Cr is mostly contained in the L_{GOE} fraction, is heavily fractionated, and is demonstrably isotopically light (-0.9 ± 0.3‰ to 1.2

449 ± 0.1‰). Mass balance calculations (section 3.4) further affirm that the isotopically light $\delta^{53}Cr$
450 composition of the bulk sediment is due to this authigenic fraction (Fig 7 and Table 3).
451
452 4.2 Cr isotope composition of detrital inputs at the SEPR
453 An appreciable component of the Cr in the SEPR sediments can be attributed to a detrital
454 source likely delivered as eolian dust. The eolian dust flux at site 598 has been estimated (Rea
455 and Bloomstine, 1986) and comprises only 0.8 – 4.0 wt% of the bulk sediment in the upper 6 m
456 of the sediment column. Our qXRD measurements verify that the mineralogy of the sediment is
457 mainly biogenic calcite and authigenic goethite, with trace amounts of albite (0 - 8%), which
458 likely represents the major mineralogical component of the eolian dust (Table 2). Albite
459 ($NaAlSi_3O_8$) is not likely to contain Cr in its crystal lattice, but we have also detected the detrital
460 spinel mineral hercynite ($Fe^{2+}Al_2O_4$), which can contain Cr(III). We find, furthermore, that an
461 appreciable amount of the total Cr in the site 598 sediment is contained in the L_{Sil} fraction (Table
462 4). Some of the Cr in our bulk L_{6NHCl} leachates is thus likely detrital rather than hydrothermal
463 and/or authigenic, and the bulk Cr isotope composition of the SEPR sediments was partly
464 inherited from eolian dust. Aluminium is typically employed as a tracer for detrital inputs to
465 many types of marine sediments, and positive correlations between Al and other elements of
466 interest have been attributed to a common detrital source (McLennan, 2001). The positive
467 correlation between Fe, Al and Cr concentrations in the SEPR sediments may thus indicate a
468 similar source for these metals, with mutual dilution by carbonate components controlling metal
469 concentrations as a function of depth. An authigenic origin for Al is also a possibility, however,
470 given that a considerable fraction (~70%) of the total Al in the sediment, as reported in (Lyle,
471 1986), is contained in the more reactive L_{HFO} and L_{GOE} sediment fractions. Correlations between
472 Cr and Al concentrations and Cr:Al ratios in our leach fractions thus cannot be solely attributed
473 to detrital contributions to the sediment, and are likely not a robust means of discriminating
474 between authigenic and detrital Cr. We further suggest that the relatively large component of
475 authigenic Al in the SEPR sediments may be hosted by authigenic clay minerals (Heath and
476 Dymond, 1977; Michalopoulos and Aller, 2004), a link needing further study at the SEPR.
477 The detrital Cr in most of the SEPR sediments carries a $\delta^{53}Cr$ indistinguishable from ISE
478 values (Fig. 7). This further shows that even though refractory Cr phases of likely detrital origin
479 comprise an appreciable proportion of the hydrothermal sediment Cr, their isotopic composition

480 is not responsible for imparting the isotopically light $\delta^{53}Cr$ composition of the bulk sediment,
481 and instead, detrital Cr effectively mutes the isotopically light authigenic Cr in measurements of
482 the bulk sediments. Our Cr:Fe ratios, furthermore, point to little Cr redistribution occurring in the
483 detrital L_{Sil} fraction (Fig. 5i). Co-variation between Cr and Fe concentrations in the L_{Sil} fraction
484 and intervals with the highest [Cr] and [Fe], however, do correspond to hercynite mineral
485 occurrences in the sediment and such correlations suggest similar origins for Cr in L_{Sil} fraction
486 and hercynite, both of which are likely supplied as eolian dust (Figure 5d and Table 2).
487 Collectively, our observations suggest that eolian dust in this part of the Pacific ocean carries the
488 $\delta^{53}Cr$ of ISE, which has remained relatively constant over the last 5.7 million years and is
489 consistent with previous studies of Cr in marine sediments (Gueguen et al., 2016; Schoenberg et
490 al., 2008).
491
492 4.3 Cr(III) oxidation in serpentinizing environments
493 The delivery of detrital Cr to the SEPR sediments (Section 4.2 above) tends to mute bulk
494 $\delta^{53}Cr$ compositions bringing them closer to the ISE, and yet, the bulk $\delta^{53}Cr$ compositions are
495 light due to an isotopically light authigenic Cr source. We thus considered whether the light
496 authigenic $\delta^{53}Cr$ recorded in the hydrothermal sediments at site 598 could have been inherited
497 directly from the hydrothermal fluids. The $\delta^{53}Cr$ composition of hydrothermal fluids is likely set
498 by alteration reactions (serpentinization) occurring within the hydrothermal vent system, and so
499 we consider whether these reactions could theoretically impart light $\delta^{53}Cr$. Two previous studies
500 that investigated the $\delta^{53}Cr$ composition of serpentinized ocean crust found it to be isotopically
501 heavy (up to +1.22‰) relative to the igneous silicate earth (ISE) (Farkas et al., 2013; Wang et
502 al., 2016). The authors interpreted these findings to be the result of a complex series of Cr redox
503 reactions, whereby seawater Cr(VI) entrained into the hydrothermal vent environment
504 experiences partial reduction in the immediate vicinity of the serpentinization site, leading to
505 isotopically heavy residual $\delta^{53}Cr(IV)$ in the hydrothermal fluids and shifting the $\delta^{53}Cr$
506 composition of any serpentinite captured Cr(III) to heavier $\delta^{53}Cr$ values. Hydrogen peroxide can
507 be present in serpentinizing systems (Oze et al., 2016), with the potential to oxidize Cr(III) and
508 thereby contribute heavy Cr(IV) to hydrothermal fluids, leaving residual serpentinites
509 isotopically light (Oze et al., 2016). Such a mechanism, however, is inconsistent with all current
510 data, which instead suggest that the net result of hydrothermal alteration processes is to produce

511 serpentinites and hydrothermal fluids with heavy $\delta^{53}Cr$ compositions ((Farkas et al., 2013; Wang
512 et al., 2016). It therefore remains unclear as to whether serpentinization reactions can generate
513 hydrothermal fluids with a light $\delta^{53}Cr$ composition and we thus consider the possible role of
514 other processes in setting the $\delta^{53}Cr$ composition of the sediments deposited at site 598.
515
516 4.4 Reduction of Cr(VI) in open vs. closed systems
517 Hydrothermal fluids provide a flux of Cr to seawater (Reinhard et al., 2013), though the
518 degree to which seawater Cr may be reduced and scavenged by hydrothermal fluids remains
519 uncertain. This means that hydrothermal systems may in fact be a net sink rather than a source of
520 Cr to seawater. To assess the extent to which Cr(III) in the SEPR sediments might originate from
521 hydrothermal vs. seawater sources we consider concentrations of Cr in vent fluids, seawater and
522 fresh plume particles. Cr(III) can be enriched in plume fluids by up to 10 times compared to
523 seawater (Sander and Koschinsky, 2000). Adopting a conservative end member Cr of 5 times
524 ambient seawater concentration (similar to measured vent fluid concentrations (Sander and
525 Koschinsky, 2000; Sander et al., 2003), would give a vent fluid Cr content of up to 50 nM Cr,
526 prior to dilution with seawater. Typical Fe concentrations in SEPR hydrothermal fluids are on
527 the order of 10 mM (Charlou et al., 1996). Using these values, the molar Cr:Fe ratio in SEPR
528 hydrothermal fluids is at most 5×10^{-6}, which is two orders of magnitude lower than the Cr:Fe
529 ratio of on axis plume particles (Feely et al., 1996) (Fig. 6) and three orders of magnitude lower
530 than the SEPR sediments at Site 598. This suggests that most Cr in hydrothermal plume particles
531 is not derived from vent fluids but rather comes from seawater in the immediate vicinity of the
532 vent, consistent with studies conducted on other hydrothermal systems (German et al., 1999;
533 Trocine and Trefry, 1988). Other estimates indeed suggest that 8 - 10% of all Cr supplied to the
534 ocean by rivers is removed via hydrothermal plume scavenging and deposited in ridge crest
535 sediments (Rudnicki and Elderfield, 1993). This suggests that scavenging of seawater Cr is a
536 non-negligible part of the global marine Cr budget, and the resulting redox reactions involved
537 may impart important isotopic effects, as we explore below.
538 Partial reduction of seawater Cr(VI) provides one likely explanation for the light $\delta^{53}Cr$
539 values we observed in the SEPR sediments. Partial reduction of seawater Cr(VI) upon mixing
540 with Fe(II) (and H_2S) laden vent fluids, and subsequent co-precipitation of Fe-(oxyhydr)oxides
541 has the potential to impart large Cr isotope fractionations, as observed in previous laboratory

experiments (Basu and Johnson, 2012; Dossing et al., 2011). While the extent to which evolving vent plumes mix with seawater, and hence how open the plume is to Cr exchange with seawater, is difficult to estimate, we consider two end-member scenarios in which Cr isotope fractionation at the SEPR results from fully open or fully closed system behaviour. A fully open, well-mixed system would most likely be achieved during reaction between Cr(VI) and Fe(II) in the water column. This would occur when the rate of mixing between seawater and the hydrothermal plume is so fast that the concentration and $\delta^{53}Cr$ composition of Cr(VI) in the latter remains the same as the former (i.e. a lack of reservoir effects). In this scenario, [Cr(VI)] and $\delta^{53}Cr$ in the plume water is constant in time and space, and the $\delta^{53}Cr$ of particles produced during seawater Cr(VI) reduction can be described by:

$$\delta^{53}Cr(III)_{product} = \delta^{53}Cr(VI)_{seawater} - \varepsilon \qquad (4)$$

where the Cr isotopic composition of seawater and the isotope fractionation factor (ε) do not change with distance from the vent.

To estimate the possible range of $\delta^{53}Cr(III)_{product}$ values, we have compiled relevant isotope fractionation factors (ε) from the literature, which span a suite of appropriate reductants for Cr(VI) in hydrothermal systems (Table 7). Under open system behaviour, the smallest fractionation factor (ε = 0.8‰), proposed by Scheiderich et al. (2015) for Cr(VI) reduction in ocean surface waters, would only yield $\delta^{53}Cr(III)_{product}$ values as light as the $\delta^{53}Cr$ observed in the SEPR sediments if the initial $\delta^{53}Cr_{seawater}$ is only mildly heavy to begin with ($\delta^{53}Cr$ = 0.13‰). Given, however, that the modern average $\delta^{53}Cr_{seawater}$ is 0.66‰, and more specifically, average Pacific ocean water is also 0.66‰ (Paulukat et al., 2016; Scheiderich et al., 2015), then Cr(VI) reduction in the SEPR system would need to be accompanied by an isotope fractionation >0.8‰ to account for the light $\delta^{53}Cr$ values in the SEPR sediments, if partial Cr(VI) reduction was exclusively responsible. Larger isotope fractionation factors, however, are expected. Dissolved ferrous iron is a potent and likely reductant of Cr(VI) in the vicinity of hydrothermal vents, as are mixed valence Fe (oxyhydr)oxides that form as direct products of Fe(II) oxidation (Table 7). Reduction of Cr(VI) by ferrous iron carries a fractionation in the range of ε = 3.6 – 4.2‰ (Dossing et al., 2011; Kitchen et al., 2012). These larger isotope fractionation factors produce

572 $\delta^{53}Cr(III)$ values lighter than our data over the entire range of known $\delta^{53}Cr_{seawater}$ compositions,
573 including the highest values measured to date ($\delta^{53}Cr_{seawater}$ = 1.24‰, Scheiderich et al. (2015)).
574 In contrast, particulate Fe(II)-bearing phases carry more muted isotope fractionation factors in
575 the range of ε = 2.11 – 2.65‰ (Table 7). Thus reduction via such particles could account for the
576 observed range of Cr isotope fractionation at the SEPR if seawater Cr(VI) had an isotopic
577 composition between $\delta^{53}Cr_{seawater}$ = 0.62 and 2.41‰, consistent with current measurements of
578 $\delta^{53}Cr_{seawater}$. Therefore, based on isotope data alone, our data can be described by partial
579 reduction of Cr(VI) in a hydrothermal system that is entirely open, using isotope fractionations
580 that fall in a continuum between 0.8‰ and 2.65‰ – magnitudes consistent with isotope
581 fractionation factors derived from laboratory experiments with a variety of ferrous Fe reductants
582 (Table 7). Variability in the isotope fractionation factor, $\delta^{53}Cr$ composition of local seawater, and
583 the extent of fluid mixing may also explain some of the variability observed in the $\delta^{53}Cr$ values
584 down core at the SEPR.
585 In contrast to a fully open system where partial Cr(VI) reduction occurs in a vigorously
586 mixed water column, a fully closed system would be approached if Cr(VI) reduction occurred
587 within the sediment pile at site 598. In this scenario, increasing burial and continued Cr(VI)
588 reduction within the sediment would drive the authigenic $\delta^{53}Cr$ of Cr(III) formed deeper in the
589 sediment towards the initial $\delta^{53}Cr$ composition of seawater at the sediment water interface. This
590 process would also tend to cause Cr:Fe ratios of the sediment to increase with depth. Neither
591 relationship is observed (Fig. 5g-h), and thus Cr(VI) reduction within the sediment pile is
592 unlikely to be the dominant process driving Cr isotope fractionation at site 598. In fact, we
593 observe the opposite relationship between sediment $\delta^{53}Cr$ composition and burial depth, finding
594 that the lightest $\delta^{53}Cr$ values measured come from samples with the lowest Cr:Fe ratios. We also
595 observe a relatively coherent relationship in which $\delta^{53}Cr$ decreases with increasing burial depth
596 and decreasing Cr:Fe ratios. We also recognize, however, that our data may fall somewhere on a
597 continuum between fully open and fully closed system behaviour, and thus record a combination
598 of water column and diagenetic Cr redox processes, the latter of which we explore below.
599
600 4.5 Diagenetic oxidation of Cr(III)

Oxidation of Cr(III) to Cr(VI) by manganese oxides has been shown under laboratory conditions ((Eary and Rai, 1987; Nakayama et al., 1981; Schroeder and Lee, 1975) and in natural soils (Oze et al., 2007), and can be described by the following reaction (Eary and Rai, 1987; Manceau and Charlet, 1992):

$$Cr^{3+} + 3MnOOH \rightarrow HCrO_4^- + 3Mn^{2+} + 2OH^- \qquad (5)$$

which produces soluble Cr(VI) oxyanions. In sediments, this Cr(VI) would be mobile and could ultimately escape by diffusion to overlying seawater. Shaw et al. (1990) determined the distribution of porewater [Cr] in the upper 20 cm of multiple continental margin sites off the coast of California, suggesting Cr loss in Mn-oxide rich surface sediments, and demonstrating low retention of Cr in sediments under oxic conditions in the presence of Mn-oxides. We observe manganese oxides throughout the sediment profile and these are present in excess of that necessary to oxidize all oxide bound Cr, based on the stoichiometry noted above. We also find the total Mn:Fe-oxide ratio decreases with distance from the ridge crest (Table 5), and this "telescoping" effect we attribute to the slower oxidation kinetics of Mn(II) with O_2 relative to Fe(II) (Dymond and Roth, 1988). Therefore, we expect more ferrous iron to be oxidized and deposited closer to the ridge crest compared to Mn, and more distal sediments, with relatively higher Mn-oxide contents, are likely to have higher potential for Cr remobilization. The diagenetic interaction of Mn-oxides with hydrothermal Cr(III) to induce oxidative remobilization as Cr(VI) is therefore a plausible and likely explanation for the apparent redistribution of Cr. Based on our current understanding of Cr isotope fractionation, and by analogy to oxidative Cr mobilization in weathering environments (Crowe et al., 2013; Frei et al., 2009; Frei and Polat, 2013), oxidatively remobilized Cr(VI) from SEPR sediments is expected to be isotopically heavier than the residual Cr(III), either due to fractionation imparted directly during oxidation (e.g., Zink et al. (2010)) or due to partial reduction back to Cr(III), which favours the light Cr isotope (Crowe et al., 2013; Ellis et al., 2002).

Chromium oxidation and remobilization from mineral phases hosting Cr(III) is dependent on the solubility of the host minerals (Rai et al., 1989). There is a progressive change in the fraction of total Fe represented in L_{HFO} and L_{GOE} at site 598 (Poulton and Canfield, 2006), and this is interpreted as a progressive transformation of reactive Fe-minerals (ferrihydrite) to more

stable phases. This is largely complete by a depth of 150 cm at site 598. We observe that the Cr:Fe molar ratio decreases steadily through the top 150 cm of sediment (Fig. 5j), which coincides with the zone of ferrihydrite transformation to goethite (Fig. 4b). Ferrihydrite transformation to goethite takes place via dissolution-reprecipitation reactions, which presumably release Cr from ferrihydrite and redistribute it to porewaters where it can be sequestered by less reactive Fe phases or become mobile through diffusive transport. Assuming a constant Cr:Fe ratio during deposition suggests progressive Cr loss relative to Fe with increasing depth in the upper 150 cm of sediment (Fig. 5j). The downcore changes suggest that Cr in ferrihydrite is redistributed into goethite by a depth of 150 cm, and that Cr loss and remobilization from ferrihydrite is complete by this depth, with less than 5% of the total Cr remaining in L_{HFO} phases (Fig. 4, Table 3). Cr(III) oxidation driven by release of Cr from L_{HFO} and subsequent reaction with Mn-oxides provides a likely explanation for the observed distribution of Cr within the upper 150 cm of the sediment and it's apparent loss from the sediment. Such a scenario is also consistent with the downcore trends in $\delta^{53}Cr$ which are strongly correlated to Cr:Fe (Fig. 7b), implying a genetic link between these two geochemical features. $\delta^{53}Cr$ values indeed become progressively lighter as Cr is lost relative to Fe, and this is consistent with the directionality of fractionation expected during oxidative Cr remobilization and the $\delta^{53}Cr$ composition of authigenic Cr captured in the L_{GOE} fraction. Thus, partial reduction of seawater Cr(VI) in the hydrothermal plume and diagenetic Cr(III) oxidation can together account for the light $\delta^{53}Cr$ values and Cr(VI) loss observed in the sediment at the SEPR.

Remobilization of Cr below 150 cm appears limited, indicating that sediments older than 2.5 Myr are poorly reactive towards Cr dissolution and consequently Cr(III) oxidation and redistribution. In these deeper sediments, Cr is dominantly hosted by goethite and residual poorly reactive detrital phases, although in other marine sediments reactive Fe phases such as ferrihydrite often convert to hematite as the stable end member (Schwertmann and Murad, 1983). At the SEPR, we expect this goethite phase to be the primary carrier of both the Cr isotope signal derived from seawater and any subsequent early diagenetic reactions, for ultimate preservation in the geologic record. Cr isotope signals imparted through partial reduction of seawater Cr(VI) and subsequently overprinted through Cr remobilization and isotope fractionation in hydrothermal sediments may thus be partly controlled by Fe (oxyhydr)oxide mineral ageing.

663 4.6 Isotopically light Cr in hydrothermal sediments

664 The light $\delta^{53}Cr$ values of the hydrothermal sediments at site 598 are unique compared to
665 most oxygenated marine sediments studied to date (Bonnand et al., 2013; Gueguen et al., 2016;
666 Reinhard et al., 2014; Wei et al., 2018). Based on our results from DSDP site 598, we argue that
667 partial reduction of seawater Cr(VI) and oxidative diagenesis combine to leave hydrothermal
668 sediments isotopically light (depleted relative to the ISE). Importantly, both of these mechanisms
669 require oxygenated seawater in the vicinity of the hydrothermal system, opening the possibility
670 that isotopically light Cr values measured in hydrothermal sediments may be diagnostic of
671 oxygen-bearing deep ocean water. In an anoxic deep ocean, Cr(III) sourced from hydrothermal
672 vents would enter seawater and precipitate in hydrothermal sediments without undergoing redox
673 cycling. The resulting hydrothermal precipitates would carry an ISE $\delta^{53}Cr$ composition (Fig. 8a).
674 In strong contrast to the anoxic deep ocean scenario, the modern oxygenated deep oceans contain
675 isotopically heavy Cr(VI), as the result of oxidative weathering on land (Frei et al., 2009, Crowe
676 et al., 2013, Scheiderich et al., 2015, D'Arcy et al., 2016, Paulukat et al., 2016, Wu et al., 2017).
677 Cr(VI) readily reacts with reductants (H_2S, Fe(II)) that accumulate in the ocean under anoxic
678 conditions, and thus Cr(VI) accumulation in the deep ocean only occurs when it is oxygenated.

679 The isotopically light signals we find in modern hydrothermal sediments develop due to
680 the local interaction of hydrothermal reductants with Cr(VI) in oxic seawater, with a possible or
681 likely partial overprint through oxidative Cr(III) diagenesis (Fig. 8b). These observations set up a
682 framework for using negative $\delta^{53}Cr$ isotope anomalies in iron oxide dominated deep-sea
683 hydrothermal sediments, as a proxy for deep-water oxygenation. Light $\delta^{53}Cr$ compositions have
684 only been observed as the result of oxidative remobilization of Cr(III) in paleosols and modern
685 soils, and in strongly oxidizing ferromanganese nodules (e.g., Crowe et al., 2013, Babechuk et al.
686 (2017); Berger and Frei (2014), Wei et al. (2018)), and here through Cr redox cycling in
687 hydrothermal plume fallout sediments. Examination of existing $\delta^{53}Cr$ records reveals
688 occurrences of isotopically light $\delta^{53}Cr$ values in Neoproterozoic hydrothermal sediments (Sial et
689 al., 2015), implying deposition from oxygenated deep ocean waters at this time. We propose that
690 this framework can be expanded through further measurements of $\delta^{53}Cr$ in older hydrothermal
691 sediments. In principle this should enable reconstruction of deep ocean oxygen dynamics
692 through geologic history.
693

5.0 Summary

Sediments deposited at the SEPR are enriched in hydrothermal Fe and Mn (oxyhydr)oxides. In the vicinity of hydrothermal vents, seawater-sourced Cr(VI) is likely reduced by Fe(II) laden vent fluids and the Cr(III) produced is scavenged by freshly-formed Fe precipitates and deposited in the sediments. This partial reduction of Cr(VI) from oxygenated seawater imparts a light $\delta^{53}Cr$ fingerprint in the plume particles, which are deposited with $\delta^{53}Cr$ values lighter than the ISE range (-0.12 ± 0.10‰). Sedimentary Mn oxides may subsequently catalyze the oxidation of sediment Cr(III), inducing the release of as much as 80% of Cr in the form of soluble Cr(VI) to the overlying water column. This remobilization may also carry an isotopic fractionation, with potential to enhance the overwhelmingly light $\delta^{53}Cr$ imparted during partial reduction. Overall, these processes combine to set a variable, but distinctly light, range in bulk sediment $\delta^{53}Cr$ of between -0.24 and -0.57‰, dictated by a heavily fractionated and isotopically light authigenic sediment fraction. The $\delta^{53}Cr$ composition of the detrital fraction of the sediment, moreover, is unfractionated and has remained relatively constant for the last 5.7 Myr. Iron diagenesis transforms less stable Fe phases (e.g., ferrihydrite) to more stable goethite by a depth of 150 cm (2.5 Myr), slowing subsequent diagenetic Fe alteration and likely locking in the $\delta^{53}Cr$ composition below this transition. Together, these processes leave a diagnostic record of isotopically light $\delta^{53}Cr$ that signals deposition from Cr(VI) bearing oxygenated deep seawater – a signal that can potentially be tracked through time, thus providing impetus to further explore ancient hydrothermal sediments as archives of $\delta^{53}Cr$ that may demarcate deep ocean oxygenation in the geologic record.

Acknowledgements

This work was funded through NSERC Discovery Grant's to SAC (0487) and RF, the Canadian Foundation for Innovation, the Canada Research Chairs Program, and the UBC 4-Year Fellowship. NJP acknowledges support from the NASA Exobiology program and Alternative Earths Astrobiology Institute. SWP acknowledges support from a Royal Society Wolfson Research Merit Award. We are grateful to Derek Vance and Rachael James for their comments on an earlier version of the manuscript.

Figure Captions

Figure 1. The modern chromium cycle, modified from Crowe et al. (2013). We display the two main Cr fluxes to the ocean, as well as the four main redox reactions, numbered in the box, that control isotope fractionation. The isotopic compositional range of each flux is provided, and it is of note that with the exception of the hydrothermal flux, all are potentially ^{53}Cr enriched. Black arrows indicate a flux of Cr that has not undergone a redox reaction, whereas grey arrows indicate a flux of Cr that has undergone a redox transformation.

Figure 2. Leach procedure schematic. **a)** Sediment extraction techniques applied in this study. The chemical extraction techniques are denoted beside each operationally defined sediment phase with the leach designation abbreviation in brackets (refer to Table 1). **b)** Sediment extraction techniques applied in Poulton and Canfield (2006) on identical sediment sections. We note that in Poulton and Canfield (2006) metal contents of the detrital silicate fraction of the sediment (Fe_{Sil}) was calculated as the difference between Fe_{TOT} and (Fe_{GOE} + Fe_{HFO}) fractions.

Figure 3. Two end member-mixing diagram. Displayed are the Cr and Fe concentrations in the L_{6NHCl} leach for samples below 250 cm, where the Cr:Fe ratio remains constant. The intercept of 0.04 ± 0.3 mg kg^{-1} provides the [Cr] expected in the carbonate phase. The dotted lines represent a 90% confidence belt on the regression.

Figure 4. Mass balance of Cr in the site 598 sediments. **a)** Concentrations of Cr in the L_{HFO}, L_{GOE} and L_{Sil} sequential leaches. We also plot the bulk Cr concentration of the sediment (L_{6NHCl} leach) **b)** Relative abundance of Cr in each sediment fraction normalized to the bulk Cr in the L_{6NHCl} leach. We note that depth intervals where [Cr] was not determined in all leach fractions (see Tables 3 and 4) have been omitted from the profiles.

Figure 5. Element concentrations at site 598. **a)** Carbonate concentration (Poulton and Canfield, 2006). **b)** Cr (blue data points) and Fe (orange data points) in the L_{HFO} fraction. **c)** Cr and Fe in the L_{GOE} fraction. **d)** Cr and Fe in the L_{Sil} fraction. **e)** Cr and Fe in the bulk L_{6NHCl} fraction. **f)** Mn-Oxide (purple) and Mn-Oxide:Fe_{6NHCl} (red data points). **g)** Cr:Fe ratio of the L_{HFO} fraction.

h) Cr:Fe ratio of the L_{GOE} fraction. **i)** Cr:Fe ratio of the L_{Sil} fraction. **j)** Cr:Fe ratio of the L_{6NHCl} fraction.

Figure 6. Cr:Fe composition of vent particles and sediments deposited at site 598. Displayed is a comparison of the Cr:Fe molar ratios of suspended vent particles measured by Feely et al. (1996), compared to the Cr:Fe composition of hydrothermal sediments at site 598 (Cr and Fe concentrations from the L_{6NHCl} leach).

Figure 7. Cr-isotope composition of sediments deposited at site 598. **a)** Cr isotope composition of the site 598 sediments. The grey shaded region represents the ISE range (-0.12 ± 0.10‰). The open diamonds represent the estimated authigenic $\delta^{53}Cr$ composition calculated using a mass balance approach (section 3.4). The closed squares represent the estimated bulk $\delta^{53}Cr$ composition calculated using a mass balance approach (section 3.4). The large errors on the mass balance obtained $\delta^{53}Cr$ values result from error propagation. **b)** Relationship between the Cr:Fe ratio and $\delta^{53}Cr$ composition of the bulk L_{6NHCl} leach for sediments deposited below 150 cm. Grey shaded region represents a 95% confidence belt on the linear regression with an r^2 value of 0.80.

Figure 8. Cr cycling in an anoxic vs. oxic deep ocean. Depicted are schematics detailing the expected $\delta^{53}Cr$ composition of hydrothermal sediments deposited in both an anoxic and oxic deep ocean. Blue arrows indicate Cr that has undergone redox cycling whereas black arrows indicate no redox state change. **a)** In a dominantly anoxic ocean, no Cr(VI) reduction takes place in the plume vicinity. This deposits unfractionated hydrothermally sourced Cr(III) in the sediment and preserves the initial ISE $\delta^{53}Cr$ composition liberated from vent efflux. **b)** In an oxygenated ocean, the heavy Cr(VI) reservoir may be partially reduced during interaction with electron donor rich hydrothermal plumes. Depending on the magnitude of the fractionation factor associated with this reaction (see Table 7), this is expected to precipitate depleted $\delta^{53}Cr$ in the sediment, making light $\delta^{53}Cr$ values diagnostic of oxygenated deep ocean waters that have interacted with hydrothermal plumes. This light $\delta^{53}Cr$ signal is only further reinforced during diagenesis with manganese oxides in the sediment pile.

818 Table 1. Summary of extraction techniques. [1](Barrett et al., 1987), [2](Poulton and Canfield, 2006),
819 [3](Thamdrup et al., 1994), [4](Poulton and Canfield, 2005), [5](Neaman et al., 2004).

Fraction designation	Sediment fraction	Extractant
	Sequential Digests	
L_{Carb}	Carbonate	10% acetic acid, 4 h[1]
L_{HFO}	Poorly crystalline hydrous ferric oxides (Fe_{HFO} in [2])	0.5 N HCl, 1 h[3]
L_{GOE}	Ferric (oxyhydr)oxides (Fe_{GOE} in [2])	0.35 M acetic acid/0.2 M Na-citrate Na-dithionite, 2 h[4]
L_{Sil}	Silicates (Fe_{Sil} in [2])	Near boiling 6 N HCl, 24 h[4]
	Bulk Sediment Digests	
L_{6NHCl}	Fe_{TOT}	Near boiling 6 N HCl, 24 h[4]
MnOx	Mn Oxides	0.1 M NH_2OH-HCl, 2 h[5]

820
821
822
823 Table 2. Mineralogical analyses of the sediments from site 598.

	Sample Depth (cm)					
	2.5	**42.5**	**75.6**	**246.5**	**398**	**499.5**
% Albite	1	2	4	8		2
% Calcite	99	85	78	56	97	83
% Goethite		11	14	33	2	15
% Hercynite		1		2	1	
% Kaolinite			2	1		
% Quartz low			2			
Total	100	100	100	100	100	100

824
825
826
827
828
829
830
831

Table 3. Element concentrations determined via sequential extractions in site 598 sediments. We note that Cr concentration of the L_{GOE} fraction was determined as the difference between total Cr (Cr_{6NHCl}, Table 4) and the sum of the sequential phases; thus $Cr_{GOE} = Cr_{6NHCl} - (Cr_{HFO} + Cr_{Sil})$. ND "Not Determined", BLD "Below Detection".

		Sequential Extractions											
	Element concentrations in L_{HFO} (0.5 N HCl) fraction			Element concentrations in L_{GOE} (Na-Dith) fraction					Element concentrations in L_{Sil} (6 N HCl)				
Depth (cm)	Cr (mg kg^{-1})	Fe (wt%)	Al (wt%)	Cr (mg kg^{-1})	Fe (wt%)	Al (wt%)	$\delta^{53}Cr$ (‰)	2se (‰)	Cr (mg kg^{-1})	Fe (wt%)	Al (wt%)	$\delta^{53}Cr$ (‰)	2se (‰)
0.5	0.3	ND	ND	ND	ND	ND	ND	ND	ND	ND	ND	ND	ND
2.5	ND	ND	ND	ND	ND	ND	ND	ND	ND	ND	ND	ND	ND
4.5	0.7	0.2	0.0	0	1.0	0.1	-1.11	0.07	0.6	0.1	0.1	-0.01	0.02
8.5	0.3	0.2	0.0	0.2	1.1	0.1	ND	ND	0.5	0.1	0.1	-0.28	0.11
21	0.3	0.3	0.1	0.3	2.4	0.1	ND	ND	1.0	0.2	0.1	-0.07	0.03
26.5	0.20	0.3	0.1	0.2	2.7	0.1	ND	ND	1.2	0.2	0.1	ND	ND
34.5	0.16	0.3	0.1	0.5	3.6	0.1	ND	ND	1.3	0.3	0.1	-0.10	0.02
42.5	0.19	0.4	0.2	0.8	5.6	0.2	ND	ND	2.1	0.5	0.2	-0.06	0.03
52.5	ND	ND	ND	ND	ND	ND	ND	ND	ND	ND	ND	ND	ND
68.5	ND	0.7	0.2	ND	7.3	0.3	ND	ND	ND	0.5	0.3	0.04	0.06
76.5	0.19	0.4	0.3	0.7	7.3	0.3	ND	ND	2.5	0.7	0.3	-0.04	0.03
84.5	0.09	0.4	0.2	0.7	6.6	0.3	-1.2	0.1	2.4	0.7	0.3	-0.06	0.03
101	0.3	0.4	0.2	0.1	5.4	0.2	ND	ND	2.2	0.3	0.2	-0.05	0.03
110.5	0.09	0.2	0.1	0.8	4.1	0.1	ND	ND	1.1	0.3	0.1	-0.06	0.03
121.5	0.08	0.2	0.1	0.3	4.0	0.1	ND	ND	1.5	0.3	0.1	-0.22	0.05
138.5	0.10	0.2	0.1	0.4	2.3	0.1	ND	ND	0.7	0.2	0.1	-0.08	0.03
150.5	0.06	0.2	0.1	0.5	3.0	0.1	-0.9	0.3	0.8	0.2	0.1	0.15	0.03
166.5	0.05	0.1	0.1	0.6	2.9	0.1	ND	ND	0.7	0.2	0.1	-0.08	0.03
186.5	0.05	0.2	0.1	0.5	3.6	0.1	ND	ND	0.7	0.2	0.1	ND	ND
196.5	0.03	0.2	0.1	0.6	4.6	0.1	-1.1	0.2	0.8	0.2	0.1	0.32	0.05
206.5	0.05	0.3	0.2	0.6	7.0	0.2	ND	ND	1.1	0.4	0.2	ND	ND
216.5	0.08	0.3	0.2	0.8	9.7	0.2	ND	ND	1.4	0.5	0.2	-0.04	0.05
236.5	0.07	0.5	0.4	0.6	12.0	0.3	ND	ND	2.0	0.7	0.3	-0.01	0.03
246.5	0.10	0.4	0.4	0.7	13.3	0.3	ND	ND	1.8	0.9	0.3	-0.03	0.03
266.5	0.05	0.4	0.3	0.9	11.7	0.2	ND	ND	1.3	0.7	0.2	-0.07	0.03
277.5	0.07	0.3	0.2	1.0	9.7	0.2	ND	ND	1.1	0.5	0.2	-0.08	0.03
286.5	0.04	0.2	0.1	0.7	6.4	0.1	ND	ND	0.7	0.3	0.1	-0.07	0.03
306.5	0.03	0.1	0.1	0.4	3.2	0.1	ND	ND	0.4	0.1	0.1	ND	ND
326.5	BLD	0.1	0.1	ND	2.3	0.0	ND	ND	0.4	0.1	0.0	ND	ND
347.5	0.05	0.2	0.1	0.7	6.1	0.1	ND	ND	0.7	0.3	0.1	-0.11	0.03
398.5	0.11	0.1	0.0	0.3	2.6	0.0	ND	ND	0.3	0.1	0.0	ND	ND
424.5	0.07	0.1	0.0	0.2	2.5	0.0	ND	ND	0.3	0.1	0.0	ND	ND

499.5	0.03	0.3	0.1	0.9	8.9	0.1	ND	ND	0.7	0.3	0.1	-0.05	0.05
549.5	0.03	0.1	0.0	0.1	1.5	0.0	ND	ND	0.3	0.0	0.0	ND	ND
Average												-0.04	0.04

837

838 Table 4. Element concentrations and Cr isotope composition determined in the bulk (L_{6NHCl}
839 leach) site 598 sediments. We note that the detrital Cr concentration was determined as the ratio
840 of Cr_{Sil} to total Cr in the Cr_{6NHCl} leach; thus % Cr detrital = (Cr_{Sil} / Cr_{6NHCl}) * 100%. ND "Not
841 Determined".

842

Bulk Sediment Leach								
Depth (cm)	**Element concentrations in L_{6NHCl} (6 N HCl)**					**Calculated Detrital fraction**	**Calculated δ^{53}Cr Authigenic (‰)**	**Calculated 2se (‰)**
	Cr (mg kg-1)	**Fe (wt%)**	**Al (wt%)**	**δ^{53}Cr (‰)**	**2se (‰)**	**Cr (%)**	**δ^{53}Cr (‰)**	**2se (‰)**
0.5	1.1	1.3	ND	-0.35	0.05	ND	ND	ND
2.5	1.2	1.2	ND	-0.37	0.05	ND	ND	ND
4.5	1.3	0.9	0.1	-0.32	0.05	0.64	-0.9	0.2
8.5	1.0	1.1	0.2	-0.33	0.05	0.53	-0.4	0.2
21	1.5	2.5	0.3	-0.3	0.05	0.64	-0.7	0.3
26.5	1.6	2.3	0.3	-0.29	0.05	0.75	ND	ND
34.5	2.0	3.7	0.5	-0.28	0.05	0.66	-0.6	0.3
42.5	3.1	4.7	0.6	-0.37	0.04	0.68	-1.0	0.2
52.5	3.2	5.5	0.7	-0.28	0.04	ND	ND	ND
68.5	3.6	6.5	0.8	-0.24	0.05	ND	ND	ND
76.5	3.4	7.2	0.9	-0.3	0.05	0.74	-1.1	0.2
84.5	3.2	6.6	0.8	-0.34	0.05	0.74	-1.1	0.2
101	2.6	4.8	0.6	-0.36	0.04	0.84	-2.0	ND
110.5	2.0	3.7	0.4	-0.34	0.05	0.57	-0.7	0.2
121.5	1.9	3.4	0.4	-0.35	0.11	0.80	-0.9	0.4
138.5	1.2	2.3	0.3	-0.27	0.06	0.56	-0.5	0.3
150.5	1.4	2.8	0.3	-0.27	0.06	0.57	-0.8	0.3
166.5	1.3	2.9	0.3	-0.28	0.05	0.52	-0.5	0.3
186.5	1.3	3.4	0.4	ND	ND	0.57	ND	ND
196.5	1.4	3.8	0.4	-0.37	0.06	0.59	-1.3	0.2
206.5	1.8	7.1	0.7	ND	ND	0.62	ND	ND
216.5	2.3	8.9	0.8	-0.38	0.05	0.60	-0.9	0.2
236.5	2.7	ND	ND	-0.5	0.04	0.75	-1.9	ND
246.5	2.6	15.0	1.4	-0.37	0.04	0.71	-1.2	0.2
266.5	2.3	11.2	1.0	-0.45	0.04	0.58	-1.0	0.2
277.5	2.1	9.1	0.8	-0.57	0.04	0.51	-1.1	0.2
286.5	1.5	6.4	0.5	-0.47	0.04	0.48	-0.8	0.2
306.5	0.9	2.8	0.2	ND	ND	0.47	ND	ND

326.5	0.8	2.6	0.2	NA	NA	0.48	ND	ND
347.5	1.4	5.7	0.5	-0.44	0.05	0.50	-0.8	0.2
398.5	0.7	2.3	0.2	ND	ND	0.48	ND	ND
424.5	0.6	2.4	0.2	ND	ND	0.50	ND	ND
499.5	1.6	7.1	0.5	-0.56	0.05	0.44	-1.0	0.2
549.5	0.4	1.2	0.1	ND	ND	0.63	ND	ND

843

844 Table 5. Mn-oxide:Fe molar ratios in the upper 20 cm of the three samples sites.

Site	Distance from ridge crest (km)	Mn:Fe Molar Ratio of Upper 20 cm
600	340	0.28
599	640	0.24
598	1130	0.39

845

846 Table 6. Compilation of modern oxic pelagic sediment and ferromanganese crust Cr isotope
847 values.

$\delta^{53}Cr_{bulk}$ (‰)	$\delta^{53}Cr_{leach}$ (‰)	2se (‰)	Reference
-0.06	NA	0.04	
0.06	NA	0.04	
-0.06	NA	0.04	
-0.06	NA	0.04	
-0.01	0.02	0.04	
-0.05	NA	0.04	
-0.07	NA	0.04	
-0.08	NA	0.04	
-0.08	NA	0.04	
-0.13	NA	0.04	
-0.14	NA	0.04	
-0.13	NA	0.04	**Gueguen et al., (2016)**
-0.08	NA	0.04	
-0.06	NA	0.04	
-0.02	NA	0.04	
-0.03	0.01	0.04	
-0.03	0.01	0.04	
-0.07	NA	0.04	
0	0.1	0.04	
0.23	NA	0.04	
0.02	NA	0.04	
-0.01	NA	0.04	
-0.1	-0.21	0.04	

	-0.11	NA	0.04	
	-0.1	NA	0.04	
	-0.016	NA	0.048	
	-0.053	NA	0.048	**Schoenberg et al., (2008)**
	-0.007	NA	0.048	
	-0.54	NA	0.03	
	-0.48	NA	0.04	
	-0.85	NA	0.04	
	-0.41	NA	0	
	-0.37	NA	0.03	
	-0.47	NA	0.04	**Wei et al., (2018)**
	-0.38	NA	0.02	
	-0.34	NA	0.02	
	-0.15	NA	0.04	
	-0.34	NA	0.03	
	-0.32	NA	0.05	
Average	**-0.15**	**-0.014**	**0.05**	

Table 7. Compilation of fraction factors during reduction of Cr(VI) adapted from Scheiderich et al., (2015).

Reference	Fractionation factor (‰)	Reductant
Scheiderich et al., (2015)	0.8‰	Organic matter in ocean surface water
Bauer et al. (2018)	1.8‰	Dissolved and solid phase Fe(II)
Basu and Johnson (2012)	3.91; 2.67; 2.65; 2.11	Goethite; siderite; green rust; FeS
Døssing et al. (2011)	3.60; 1.50	Ferrous Fe; 'Green rust'
Ellis et al. (2002)	3.51	Magnetite
Kitchen et al. (2012)	4.20; 3.11	Low-pH Fe(II); organic reductants
Sikora et al. (2008)	4.11; 1.75	*Shewanella oneidensis* bacteria
Zink et al. (2010)	3.54; 5.0	Acidic H_2O_2; pH-neutral H_2O_2 (kinetic)

REFERENCES

Babechuk, M.G., Kleinhanns, I.C., Schoenberg, R., 2017. Chromium geochemistry of the ca. 1.85 Ga Flin Flon paleosol. Geobiology, 15(1): 30-50.

Barrett, T.J., Taylor, P.N., Lugowski, J., 1987. Metalliferous sediments from DSDP Leg 92: The East Pacific Rise transect. Geochimica Et Cosmochimica Acta, 51(9): 2241-2253.

Basu, A., Johnson, T.M., 2012. Determination of Hexavalent Chromium Reduction Using Cr Stable Isotopes: Isotopic Fractionation Factors for Permeable Reactive Barrier Materials. Environmental Science & Technology, 46(10): 5353-5360.

Bauer, K.W. et al., 2018. Chromium isotope fractionation in ferruginous sediments. Geochimica et Cosmochimica Acta, 223: 198-215.

Berger, A., Frei, R., 2014. The fate of chromium during tropical weathering: A laterite profile from Central Madagascar. Geoderma, 213: 521-532.

Bonnand, P., James, R.H., Parkinson, I.J., Connelly, D.P., Fairchild, I.J., 2013. The chromium isotopic composition of seawater and marine carbonates. Earth and Planetary Science Letters, 382: 10-20.

Chao, T.T., 1972. Selective Dissolution of Manganese Oxides from Soils and Sediments with Acidified Hydroxylamine Hydrochloride. Soil Science Society of America Proceedings, 36(5): 764-&.

Charlou, J.L. et al., 1996. Mineral and gas chemistry of hydrothermal fluids on an ultrafast spreading ridge: East Pacific Rise, 17 degrees to 19 degrees S (Naudur cruise, 1993) phase separation processes controlled by volcanic and tectonic activity. Journal of Geophysical Research-Solid Earth, 101(B7): 15899-15919.

Cole, D.B. et al., 2016. A shale-hosted Cr isotope record of low atmospheric oxygen during the Proterozoic. Geology, 44(7): 555-558.

Crowe, S.A. et al., 2013. Atmospheric oxygenation three billion years ago. Nature, 501(7468): 535-+.

D'Arcy, J., Babechuk, M.G., Dossing, L.N., Gaucher, C., Frei, R., 2016. Processes controlling the chromium isotopic composition of river water: Constraints from basaltic river catchments. Geochimica Et Cosmochimica Acta, 186: 296-315.

Davis, J.A., Leckie, J.O., 1980. Surface ionization and complexation at the oxide/water interface. 3. Adsorption of anions. Journal of Colloid and Interface Science, 74(1): 32-43.

Dossing, L.N., Dideriksen, K., Stipp, S.L.S., Frei, R., 2011. Reduction of hexavalent chromium by ferrous iron: A process of chromium isotope fractionation and its relevance to natural environments. Chemical Geology, 285(1-4): 157-166.

Dymond, J., Roth, S., 1988. Plume dispersed hydrothermal particles: A time-series record of settling flux from the Endeavour Ridge using moored sensors. Geochimica Et Cosmochimica Acta, 52(10): 2525-2536.

Eary, L.E., Rai, D., 1987. Kinetics of chromium(III) oxidation to chromium(VI) by reaction with manganese dioxide. Environmental Science & Technology, 21(12): 1187-1193.

Ellis, A.S., Johnson, T.M., Bullen, T.D., 2002. Chromium isotopes and the fate of hexavalent chromium in the environment. Science, 295(5562): 2060-2062.

Farkas, J. et al., 2013. Chromium isotope variations (delta Cr-53/52) in mantle-derived sources and their weathering products: Implications for environmental studies and

the evolution of delta Cr-53/52 in the Earth's mantle over geologic time. Geochimica Et Cosmochimica Acta, 123: 74-92.
Feely, R.A. et al., 1996. Hydrothermal plume particles and dissolved phosphate over the superfast-spreading southern East Pacific Rise. Geochimica Et Cosmochimica Acta, 60(13): 2297-2323.
Fendorf, S.E., 1995. Surface reactions of chromium in soils and waters. Geoderma, 67(1-2): 55-71.
Frei, R., Gaucher, C., Dossing, L.N., Sial, A.N., 2011. Chromium isotopes in carbonates - A tracer for climate change and for reconstructing the redox state of ancient seawater. Earth and Planetary Science Letters, 312(1-2): 114-125.
Frei, R., Gaucher, C., Poulton, S.W., Canfield, D.E., 2009. Fluctuations in Precambrian atmospheric oxygenation recorded by chromium isotopes. Nature, 461(7261): 250.
Frei, R., Polat, A., 2013. Chromium isotope fractionation during oxidative weathering-Implications from the study of a Paleoproterozoic (ca. 1.9 Ga) paleosol, Schreiber Beach, Ontario, Canada. Precambrian Research, 224: 434-453.
German, C.R., Hergt, J., Palmer, M.R., Edmond, J.M., 1999. Geochemistry of a hydrothermal sediment core from the OBS vent-field, 21 degrees N East Pacific Rise. Chemical Geology, 155(1-2): 65-75.
Gilleaudeau, G.J. et al., 2016. Oxygenation of the mid-Proterozoic atmosphere: clues from chromium isotopes in carbonates. Geochemical Perspectives Letters, 2(2): 178-+.
Gueguen, B. et al., 2016. The chromium isotope composition of reducing and oxic marine sediments. Geochimica Et Cosmochimica Acta, 184: 1-19.
Heath, G.R., Dymond, J., 1977. Genesis and transformation of metalliferous sediments from the East Pacific Rise, Bauer Deep, and Central Basin, northwest Nazca plate. Geological Society of America Bulletin, 88(5): 723-733.
Holmden, C., Jacobson, A.D., Sageman, B.B., Hurtgen, M.T., 2016. Response of the Cr isotope proxy to Cretaceous Ocean Anoxic Event 2 in a pelagic carbonate succession from the Western Interior Seaway. Geochimica Et Cosmochimica Acta, 186: 277-295.
Jeandel, C., Minster, J.F., 1984. Isotope dilution measurement of inorganic chromium(III) and total chromium in seawater. Marine Chemistry, 14(4): 347-364.
Kitchen, J.W., Johnson, T.M., Bullen, T.D., Zhu, J., Raddatz, A., 2012. Chromium isotope fractionation factors for reduction of Cr(VI) by aqueous Fe(II) and organic molecules. Geochimica Et Cosmochimica Acta, 89: 190-201.
Konhauser, K.O. et al., 2011. Aerobic bacterial pyrite oxidation and acid rock drainage during the Great Oxidation Event. Nature, 478(7369): 369-+.
Lyle, M.W., 1986. Major element composition of Leg 92 sediments (East Pacific Rise). Initial Reports of the Deep Sea Drilling Project, 92: 355-370.
Manceau, A., Charlet, L., 1992. X-ray absorption spectroscopic study of the sorption of Cr(III) at the oxide-water interface: I. Molecular mechanism of Cr(III) oxidation on Mn oxides. Journal of Colloid and Interface Science, 148(2): 425-442.
McClain, C.N., Maher, K., 2016. Chromium fluxes and speciation in ultramafic catchments and global rivers. Chemical Geology, 426: 135-157.
McLennan, S.M., 2001. Relationships between the trace element composition of sedimentary rocks and upper continental crust. Geochemistry Geophysics Geosystems, 2: art. no.-2000GC000109.

Michalopoulos, P., Aller, R.C., 2004. Early diagenesis of biogenic silica in the Amazon delta: Alteration, authigenic clay formation, and storage. Geochimica Et Cosmochimica Acta, 68(5): 1061-1085.
Nakayama, E., Kuwamoto, T., Tsurubo, S., Fujinaga, T., 1981. Chemical speciation of chromium in sea water: Part 2. Effects of Manganese Oxides and Reducible Organic Materials on the Redox Processes of Chromium. Analytica Chimica Acta, 130(2): 401-404.
Neaman, A., Waller, B., Mouele, F., Trolard, F., Bourrie, G., 2004. Improved methods for selective dissolution of manganese oxides from soils and rocks. European Journal of Soil Science, 55(1): 47-54.
Oze, C., Bird, D.K., Fendorf, S., 2007. Genesis of hexavalent chromium from natural sources in soil and groundwater. Proceedings of the National Academy of Sciences of the United States of America, 104(16): 6544-6549.
Oze, C., Fendorf, S., Bird, D.K., Coleman, R.G., 2004. Chromium geochemistry in serpentinized ultramafic rocks and serpentine soils from the Franciscan Complex of California. American Journal of Science, 304(1): 67-101.
Oze, C., Sleep, N.H., Coleman, R.G., Fendorf, S., 2016. Anoxic oxidation of chromium. Geology, 44(7): 543-546.
Paulukat, C., Gilleaudeau, G.J., Chernyavskiy, P., Frei, R., 2016. The Cr-isotope signature of surface seawater—a global perspective. Chemical Geology, 444: 101-109.
Planavsky, N.J. et al., 2014. Low Mid-Proterozoic atmospheric oxygen levels and the delayed rise of animals. Science, 346(6209): 635-638.
Poulton, S.W., Canfield, D.E., 2005. Development of a sequential extraction procedure for iron: implications for iron partitioning in continentally derived particulates. Chemical Geology, 214(3-4): 209-221.
Poulton, S.W., Canfield, D.E., 2006. Co-diagenesis of iron and phosphorus in hydrothermal sediments from the southern East Pacific Rise: Implications for the evaluation of paleoseawater phosphate concentrations. Geochimica Et Cosmochimica Acta, 70(23): 5883-5898.
Rai, D., Eary, L.E., Zachara, J.M., 1989. Environmental chemistry of chromium. Science of the Total Environment, 86(1-2): 15-23.
Rea, D.K., Bloomstine, M.K., 1986. Neogene history of the South Pacific tradewinds: evidence for hemispherical asymmetry of atmospheric circulation. Palaeogeography, palaeoclimatology, palaeoecology, 55(1): 55-64.
Reinhard, C.T. et al., 2013. Proterozoic ocean redox and biogeochemical stasis. Proceedings of the National Academy of Sciences of the United States of America, 110(14): 5357-5362.
Reinhard, C.T. et al., 2014. The isotopic composition of authigenic chromium in anoxic marine sediments: A case study from the Cariaco Basin. Earth and Planetary Science Letters, 407: 9-18.
Rudnicki, M.D., Elderfield, H., 1993. A chemical model of the buoyant and neutrally buoyant plume above the TAG vent field, 26 degrees N, Mid-Atlantic Ridge. Geochimica Et Cosmochimica Acta, 57(13): 2939-2957.
Saad, E.M., Wang, X.L., Planavsky, N.J., Reinhard, C.T., Tang, Y.Z., 2017. Redox-independent chromium isotope fractionation induced by ligand-promoted dissolution. Nature Communications, 8.

989 Sander, S., Koschinsky, A., 2000. Onboard-ship redox speciation of chromium in diffuse
990 hydrothermal fluids from the North Fiji Basin. Marine Chemistry, 71(1-2): 83-102.
991 Sander, S., Koschinsky, A., Halbach, P., 2003. Redox speciation of chromium in the oceanic
992 water column of the Lesser Antilles and offshore Otago Peninsula, New Zealand.
993 Marine and Freshwater Research, 54(6): 745-754.
994 Scheiderich, K., Amini, M., Holmden, C., Francois, R., 2015. Global variability of chromium
995 isotopes in seawater demonstrated by Pacific, Atlantic, and Arctic Ocean samples.
996 Earth and Planetary Science Letters, 423: 87-97.
997 Schoenberg, R., Zink, S., Staubwasser, M., von Blanckenburg, F., 2008. The stable Cr isotope
998 inventory of solid Earth reservoirs determined by double spike MC-ICP-MS.
999 Chemical Geology, 249(3-4): 294-306.
1000 Schroeder, D.C., Lee, G.F., 1975. Potential transformations of chromium in natural waters.
1001 Water Air and Soil Pollution, 4(3-4): 355-365.
1002 Schwertmann, U., Murad, E., 1983. Effect of pH on the formation of goethite and hematite
1003 from ferrihydrite. Clays and Clay Minerals, 31(4): 277-284.
1004 Shaw, T.J., Gieskes, J.M., Jahnke, R.A., 1990. Early diagenesis in differing depositional
1005 environments: The response of transition metals in pore water. Geochimica Et
1006 Cosmochimica Acta, 54(5): 1233-1246.
1007 Sial, A.N. et al., 2015. Algoma-type Neoproterozoic BIFs and related marbles in the Serido
1008 Belt (NE Brazil): REE, C, O, Cr and Sr isotope evidence. Journal of South American
1009 Earth Sciences, 61: 33-52.
1010 Siebert, C., Nagler, T.F., Kramers, J.D., 2001. Determination of molybdenum isotope
1011 fractionation by double-spike multicollector inductively coupled plasma mass
1012 spectrometry. Geochemistry Geophysics Geosystems, 2: 1032.
1013 Thamdrup, B., Fossing, H., Jorgensen, B.B., 1994. Manganese, iron and sulfur cycling in a
1014 coastal marine sediment, Aarhus Bay, Denmark. Geochimica Et Cosmochimica Acta,
1015 58(23): 5115-5129.
1016 Trocine, R.P., Trefry, J.H., 1988. Distribution and chemistry of suspended particles from an
1017 active hydrothermal vent site on the Mid-Atlantic Ridge at 26°N. Earth and
1018 Planetary Science Letters, 88(1-2): 1-15.
1019 Wang, X.L. et al., 2017. Chromium isotopic composition of core-top planktonic foraminifera.
1020 Geobiology, 15(1): 51-64.
1021 Wang, X.L. et al., 2016. Chromium isotope fractionation during subduction-related
1022 metamorphism, black shale weathering, and hydrothermal alteration. Chemical
1023 Geology, 423: 19-33.
1024 Wei, W. et al., 2018. Marine ferromanganese oxide: A potentially important sink of light
1025 chromium isotopes? Chemical Geology.
1026 Wiederhold, J.G. et al., 2006. Iron isotope fractionation during proton-promoted, ligand-
1027 controlled, and reductive dissolution of goethite. Environmental science &
1028 technology, 40(12): 3787-3793.
1029 Wu, W.H., Wang, X.L., Reinhard, C.T., Planaysky, N.J., 2017. Chromium isotope systematics in
1030 the Connecticut River. Chemical Geology, 456: 98-111.
1031 Yusof, A.M., Chia, C.H., Wood, A.K.H., 2007. Speciation of Cr(III) and Cr(VI) in surface waters
1032 with a Chelex-100 resin column and their quantitative determination using
1033 inductively coupled plasma mass spectrometry and instrumental neutron activation
1034 analysis. Journal of Radioanalytical and Nuclear Chemistry, 273(3): 533-538.

Zink, S., Schoenberg, R., Staubwasser, M., 2010. Isotopic fractionation and reaction kinetics between Cr(III) and Cr(VI) in aqueous media. Geochimica Et Cosmochimica Acta, 74(20): 5729-5745.

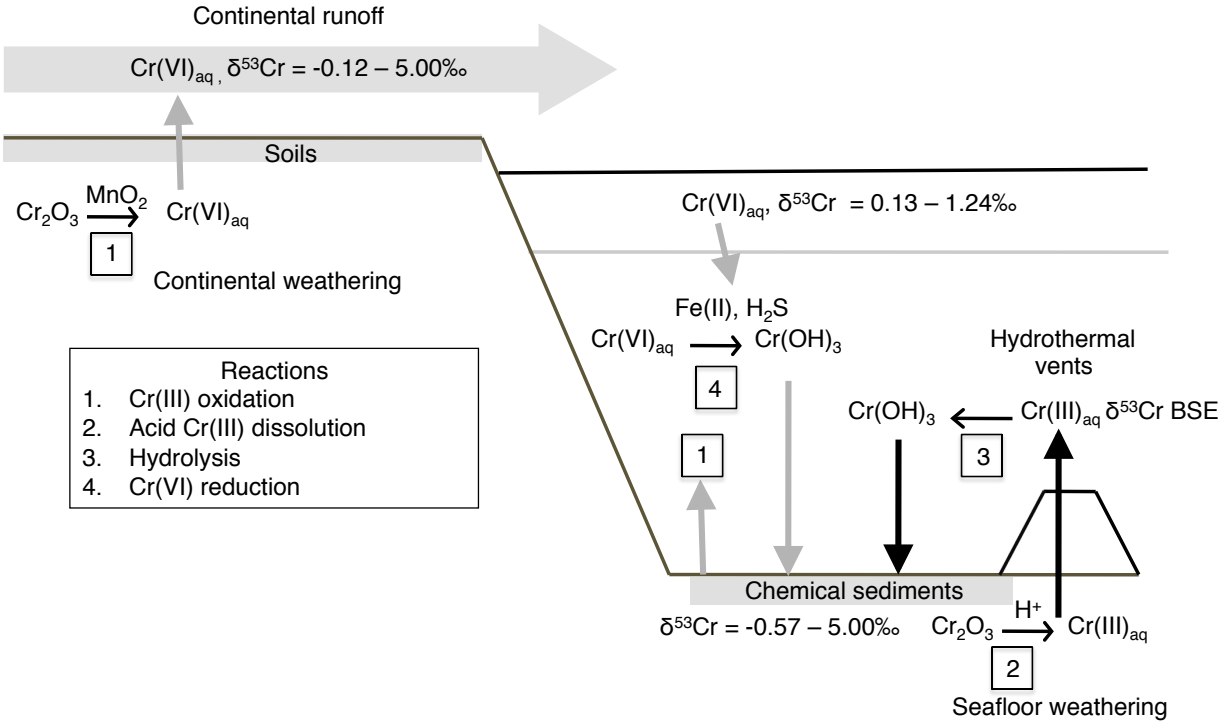
Continental runoff
Cr(VI)aq , δ53Cr = -0.12 – 5.00‰
Soils
Cr2O3 MnO2 Cr(VI)aq
1
Continental weathering
Reactions
1. Cr(III) oxidation
2. Acid Cr(III) dissolution
3. Hydrolysis
4. Cr(VI) reduction
Cr(VI)aq, δ53Cr = 0.13 – 1.24‰
Fe(II), H2S
Cr(VI)aq Cr(OH)3
4
1
Hydrothermal vents
Cr(OH)3
Cr(III)aq δ53Cr BSE
3
Chemical sediments
δ53Cr = -0.57 – 5.00‰
Cr2O3 H+ Cr(III)aq
2
Seafloor weathering

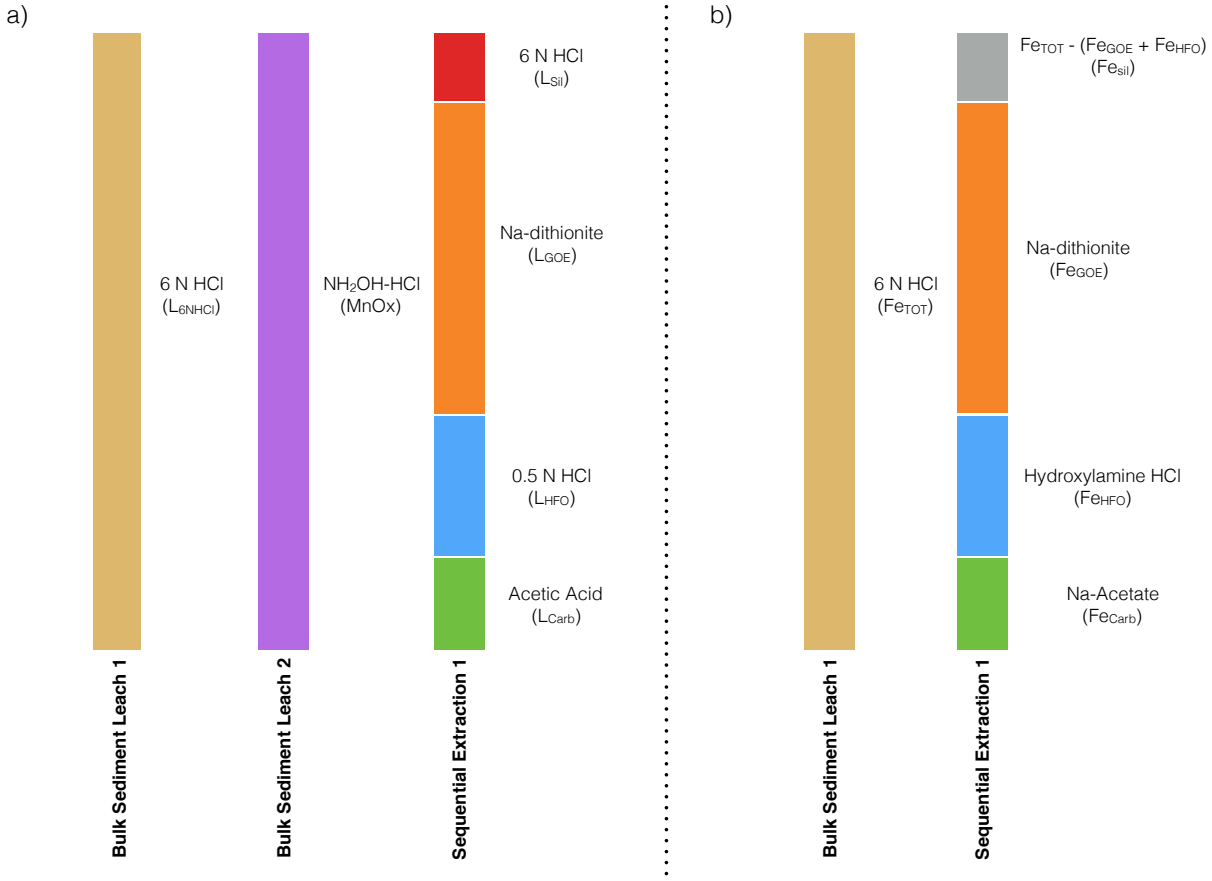
a)
6 N HCl
(L_{6NHCl})
NH_2OH-HCl
(MnOx)
6 N HCl
(L_{SII})
Na-dithionite
(L_{GOE})
0.5 N HCl
(L_{HFO})
Acetic Acid
(L_{Carb})
Bulk Sediment Leach 1
Bulk Sediment Leach 2
Sequential Extraction 1
b)
6 N HCl
(Fe_{TOT})
Fe_{TOT} - (Fe_{GOE} + Fe_{HFO})
(Fe_{sil})
Na-dithionite
(Fe_{GOE})
Hydroxylamine HCl
(Fe_{HFO})
Na-Acetate
(Fe_{Carb})
Bulk Sediment Leach 1
Sequential Extraction 1

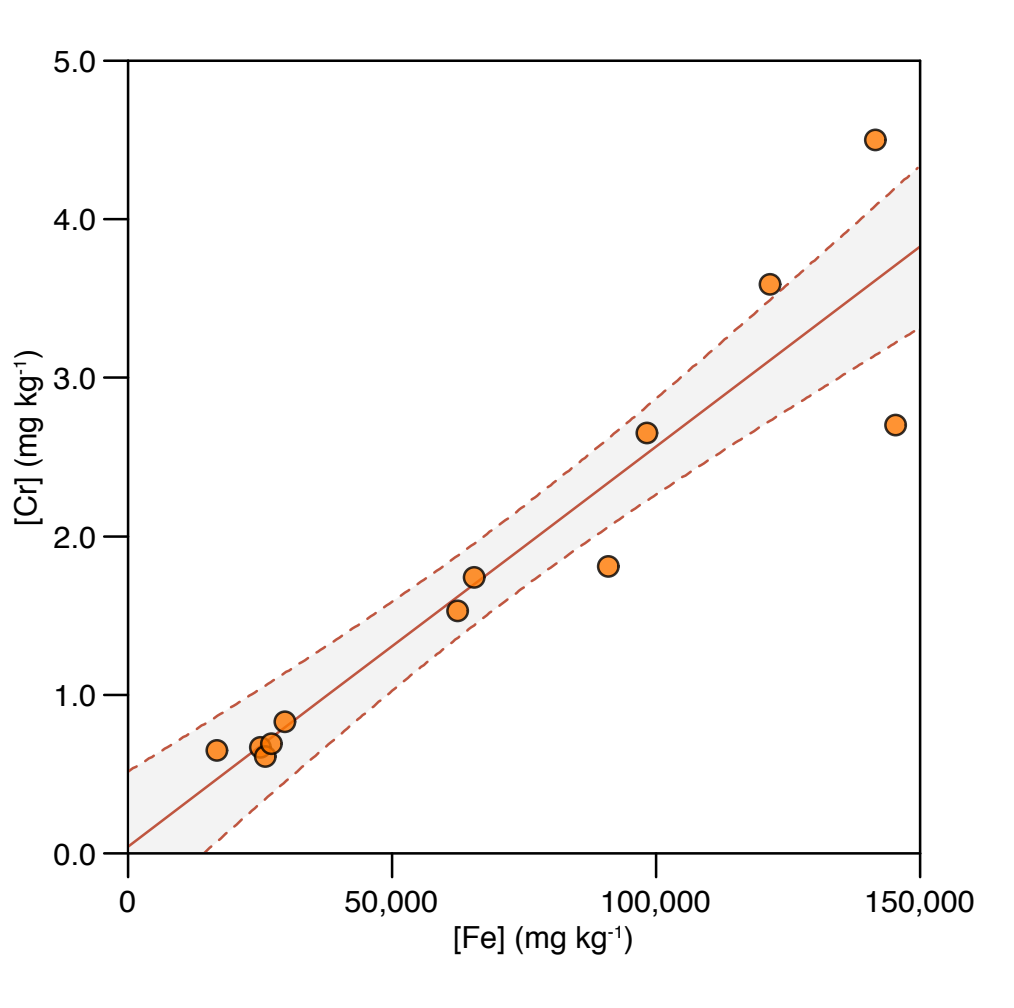
5.0
4.0
3.0
2.0
1.0
0.0
[Cr] (mg kg-1)
0
50,000
100,000
150,000
[Fe] (mg kg-1)

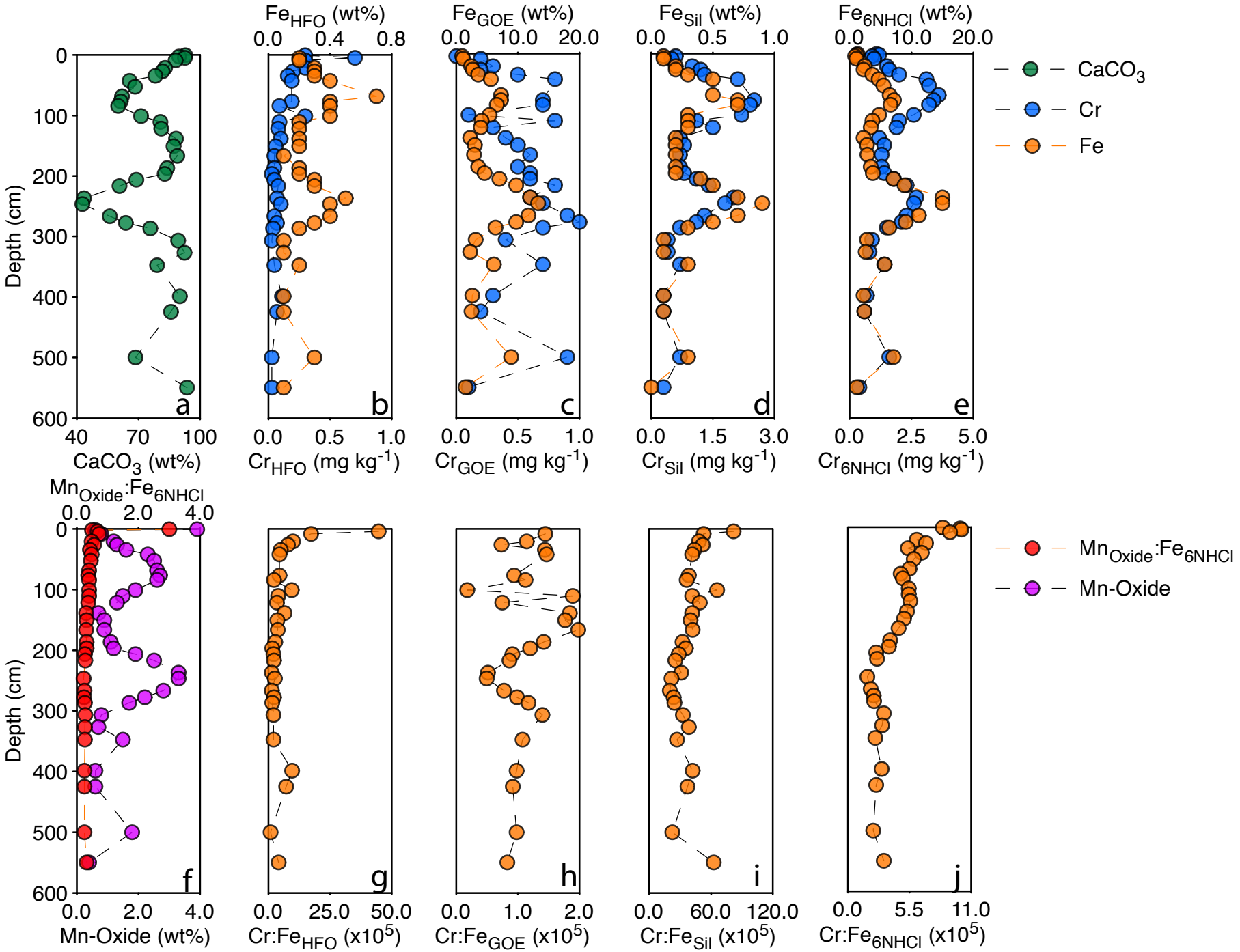
Depth (cm)
0
100
200
300
400
500
600
a
40
70
100
CaCO3 (wt%)
FeHFO (wt%)
0.0
0.4
0.8
b
0.0
0.5
1.0
CrHFO (mg kg-1)
FeGOE (wt%)
0.0
10.0
20.0
c
0.0
0.5
1.0
CrGOE (mg kg-1)
FeSil (wt%)
0.0
0.5
1.0
d
0.0
1.5
3.0
CrSil (mg kg-1)
Fe6NHCl (wt%)
0.0
10.0
20.0
e
0.0
2.5
5.0
Cr6NHCl (mg kg-1)
CaCO3
Cr
Fe
MnOxide:Fe6NHCl
0.0
2.0
4.0
f
0.0
2.0
4.0
Mn-Oxide (wt%)
g
0.0
25.0
50.0
Cr:FeHFO (x10^5)
h
0.0
1.0
2.0
Cr:FeGOE (x10^5)
i
0.0
60.0
120.0
Cr:FeSil (x10^5)
j
0.0
5.5
11.0
Cr:Fe6NHCl (x10^5)
MnOxide:Fe6NHCl
Mn-Oxide

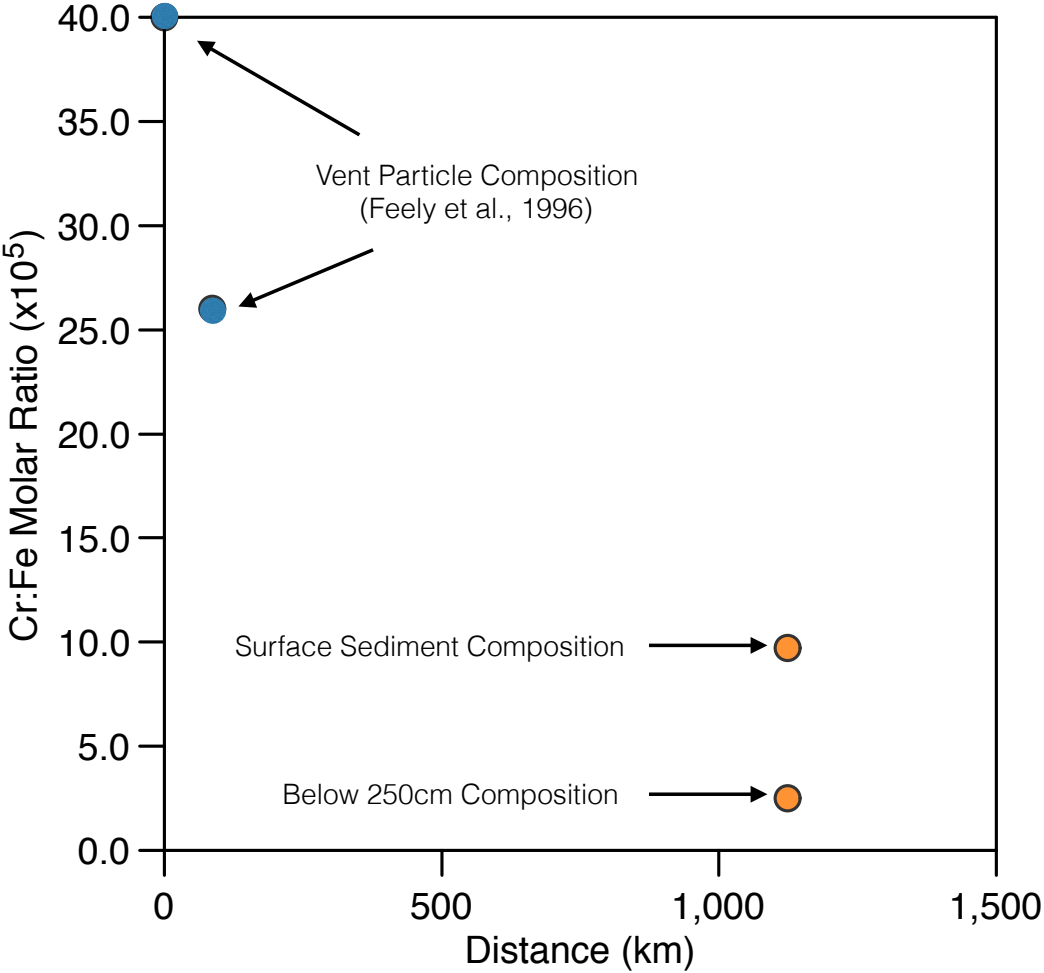
40.0
35.0
30.0
25.0
20.0
15.0
10.0
5.0
0.0
Cr:Fe Molar Ratio (x10^5)
Vent Particle Composition
(Feely et al., 1996)
Surface Sediment Composition
Below 250cm Composition
0
500
1,000
1,500
Distance (km)

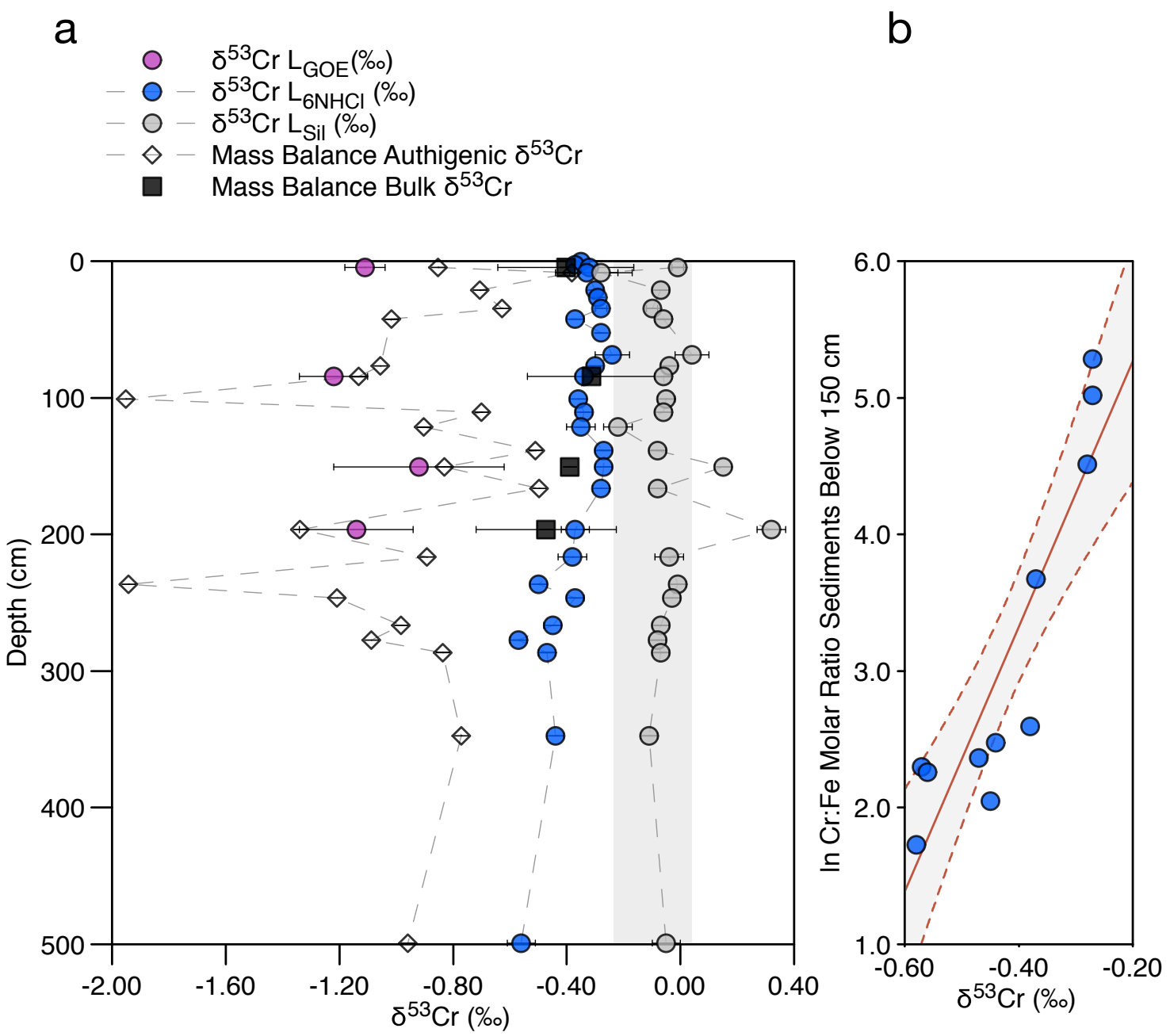
a
b
δ53Cr LGOE(‰)
δ53Cr L6NHCl (‰)
δ53Cr LSil (‰)
Mass Balance Authigenic δ53Cr
Mass Balance Bulk δ53Cr
Depth (cm)
0
100
200
300
400
500
-2.00
-1.60
-1.20
-0.80
-0.40
0.00
0.40
δ53Cr (‰)
ln Cr:Fe Molar Ratio Sediments Below 150 cm
6.0
5.0
4.0
3.0
2.0
1.0
-0.60
-0.40
-0.20
δ53Cr (‰)

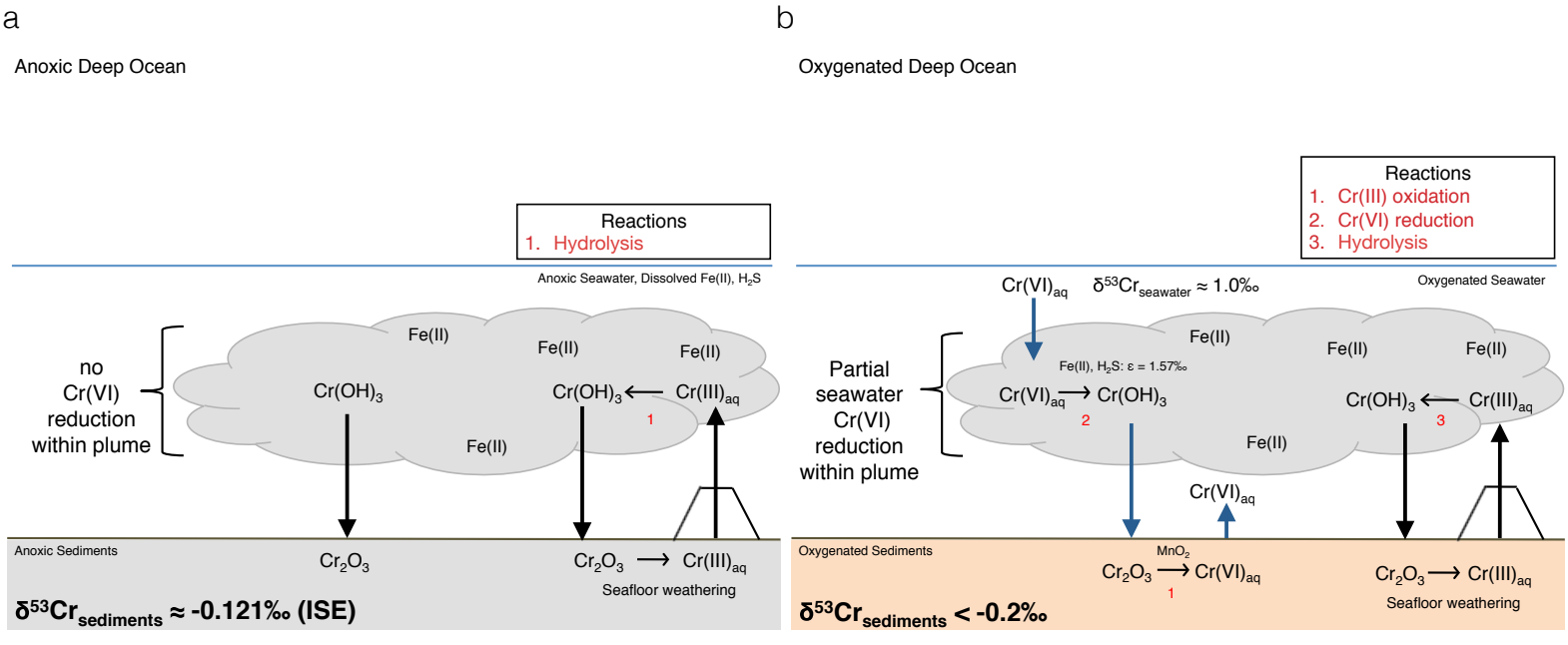
a
Anoxic Deep Ocean
Reactions
1. Hydrolysis
Anoxic Seawater, Dissolved Fe(II), H2S
no Cr(VI) reduction within plume
Fe(II)
Fe(II)
Fe(II)
Fe(II)
Cr(OH)3
Cr(OH)3 ← Cr(III)aq
1
Anoxic Sediments
Cr2O3
Cr2O3 → Cr(III)aq
Seafloor weathering
δ53Crsediments ≈ -0.121‰ (ISE)
b
Oxygenated Deep Ocean
Reactions
1. Cr(III) oxidation
2. Cr(VI) reduction
3. Hydrolysis
Cr(VI)aq
δ53Crseawater ≈ 1.0‰
Oxygenated Seawater
Partial seawater Cr(VI) reduction within plume
Fe(II)
Fe(II)
Fe(II)
Fe(II), H2S: ε = 1.57‰
Cr(VI)aq → Cr(OH)3
2
Cr(OH)3 ← Cr(III)aq
3
Fe(II)
Cr(VI)aq
Oxygenated Sediments
MnO2
Cr2O3 → Cr(VI)aq
1
Cr2O3 → Cr(III)aq
Seafloor weathering
δ53Crsediments < -0.2‰